

Cancer-associated Bax point mutations block apoptotic pore formation by trapping kinetic intermediates

Justin Kale^{1*}, John A. Bachman^{3*}, Brian Leber⁴, Peter Sorger³, David Andrews^{1,2,4}

Sunnybrook Research Institute¹ and Department of Medical Biophysics², University of Toronto; Laboratory of Systems Pharmacology³, Harvard Medical School; Departments of Biomedical Sciences⁴ and Biochemistry and Medicine⁵, McMaster University

* Authors contributed equally

Abstract

The key checkpoint in apoptosis is mitochondrial outer membrane permeabilization (MOMP), which involves activation and oligomerization of Bax and Bak to form transmembrane pores. Caspase activation and cell death then ensue. Although pore formation is highly dynamic, current understanding of Bax and Bak is based on analysis of equilibrium structures, resulting in multiple competing models. To understand this key step in apoptosis we used mechanistic mathematical modeling to analyze kinetic data on protein-protein interaction, protein-membrane insertion and membrane permeabilization obtained from a fully reconstituted system. We find that Bax activation involves two discrete steps. In the first, Bax interacts with BH3-only activator protein and partially inserts into the membrane; in a subsequent and slower step, Bax oligomerizes to form pores. Bax mutations found in human tumors trap the protein in the proposed intermediate state demonstrating its role as an essential step in pore formation.

Main

Mitochondrial outer membrane permeabilization (MOMP) triggers apoptosis and is regulated by Bcl-2 family proteins^{1,2}. MOMP occurs when the pro-apoptotic Bcl-2 proteins Bax and Bak are activated and undergo a series of conformation changes resulting in homo-oligomerization in the outer mitochondrial membrane. Pores made up of Bax and Bak facilitate the release of pro-apoptotic proteins, such as cytochrome *c* and SMAC, from the intermembrane space into the cytosol, resulting in the activation of a caspase cascade that triggers the degradation of cellular components and irreversible progression to cell death^{3,4}. Thus the activation status of Bax and Bak is a key apoptosis regulator and determinant of cell fate⁵⁻⁷.

Bax has been extensively studied and a variety of models have been proposed to explain the mechanisms by which Bax becomes activated and the structure it forms at the membrane. Although these models differ, there is strong consensus about several critical steps: (1) the $\alpha 9$ helix is inserted into the bilayer; (2) Bax dimerization is initiated by interactions with activator BH3 proteins such as Bid and Bim; and (3) Bax homodimer formation is mediated by the symmetric binding of the BH3-motif in the $\alpha 2$ helix

of one Bax to the hydrophobic BH3-binding groove ($\alpha 2-4$) of another (Figure 1a)⁸. There is also agreement that the amphipathic $\alpha 5$ and $\alpha 6$ helices lie in-plane with the membrane and/or line the Bax pore when inserted into the outer membrane. Areas of uncertainty include the following: (1) whether BH3 proteins activate Bax via the ‘rear’ or ‘front’ pocket; (2) whether different BH3 proteins cause Bax to undergo different activation pathways as implied by interaction with different binding sites; (3) whether there exist temporally distinct conformations of Bax intermediate between soluble monomers and the final membrane embedded oligomer; and (4) whether the $\alpha 9$ helix is inserted into the membrane before the rest of the protein inserts and oligomerizes within the bilayer. In general, static or equilibrium measurements have provided the most useful insight into the structure of assembled pores but have been less informative about intermediate conformations⁹⁻¹³. Conversely, kinetic studies have clarified aspects of the sequence of steps but lack structural information about conformational states¹⁴⁻¹⁶. An assay that dynamically tracks the structural features of Bax conformation changes over time is required to unify kinetic and structural insight.

In this paper we delineate the conformational rearrangements during Bax activation by applying fluorescence spectroscopy and kinetic modeling to an *in vitro* reconstituted system involving liposomes and full-length recombinant proteins. We labelled Bax at 19 different residues using an environmentally sensitive dye that reports on hydrophobicity in the local environment of each label, and simultaneously measured intermolecular FRET to determine the timing of protein-protein interactions relative to Bax conformation changes. The resulting data were used to calibrate kinetic models involving ordinary differential equations (ODEs) that described the number and timing of conformation changes at each labeled residue. The Bax conformations we identified as associated with activation include a monomer (C_0) that transitions rapidly to a membrane-associated intermediate (C_1) involved in binding to BH3 activators, followed by a slower transition to a conformation (C_2) associated with full insertion into the membrane and subsequent oligomerization to form pores. We validate the existence of the proposed C_1

state by assaying point mutants found in human cancer and cancer cell lines and identify several that trap Bax in the C₁ intermediate, thereby inhibiting membrane permeabilization.

Results

To label Bax at multiple sites, single cysteine mutants were expressed, purified and labelled with the thiol-reactive fluorophore NBD-maleimide^{15,17} (Figure 1b). The peak fluorescence intensity of NBD depends on local hydrophobicity and it has therefore been used previously to study membrane protein conformation^{9,13,15,18,19}. NBD was added at locations in Bax that made it possible to monitor nine different helices; these locations spanned the N-terminus, BH3-binding groove, pore-forming helices (α 5 and α 6), and C-terminus (α 9). Formation of Bax-containing pores was initiated by addition of recombinant cBid and Bim, and pore formation was monitored using liposomes loaded with a fluorescent terbium-dipicolinic acid complex (Tb:DPA). When Bax permeabilizes the liposomes, Tb:DPA is released and fluorescence falls due to chelation of Tb by EDTA present in the buffer (Figure 1c)^{15,17}. The fluorescence of Tb:DPA and NBD are spectrally distinct, permitting simultaneous measurement of Bax conformational changes and pore formation in real time.

Bax undergoes extensive conformation changes during activation

The *fold-change* in NBD fluorescence upon Bax activation, $(F/F_0 = \frac{F_{end\ of\ assay} - background}{F_{start\ of\ assay} - background})$, reports on the difference in the local environment of a residue in aqueous and membrane-bound states (Figure 2a); a value >1 denotes an increase in hydrophobicity and <1 denotes a decrease. One hour after addition of a BH3 activator we found that multiple residues experienced large changes in relative fluorescence; these changes were similar in magnitude when activation was triggered by cBid or Bim. Overall 10 labelled residues underwent a transition to a more hydrophobic environment, 8 were relatively unchanged ($1 < F/F_0 < 2$) and one residue (number 47) moved to a more hydrophilic environment (Figure 2a). All labelled Bax proteins were also active in permeabilizing liposomes (Figure S1a) but the kinetics

varied widely (Figure S1b). From these data we conclude that widespread rearrangements of Bax occur during pore formation.

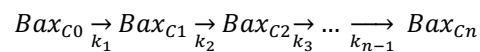
With respect to time, NBD fluorescence trajectories for labelled Bax residues fell into two classes depending on location within the protein (Figure 2b). Most residues exhibited monotonic increases in fluorescence similar to those we have previously reported for Bax-126C-NBD¹⁵. However, rates of fluorescence change varied within this class, with some labelled residues rapidly approaching a steady state fluorescence value (e.g., residue 3) and others (residue 120) changing more slowly (Figure 2b). A second class comprised four residues in the BH3-binding groove (54, 62, 68 and 79) that exhibited a rapid increase in fluorescence, followed by a more gradual decline towards the steady state fluorescence value (residues 54, 68 and 79) or – alternatively - a slower monotonic increase (residue 62) (Figure 2b).

We aimed to establish a Bax membrane insertion “pathway” by determining the relative timing of conformational changes for different regions of the protein. However, we anticipated that the addition of NBD labels to different sites on Bax would alter the overall rate of Bax activation (Figure S1b), simultaneously affecting the timing of NBD fluorescence changes and pore formation. To assess the degree to which observed residue by residue variation in NBD fluorescence dynamics was attributable to differences in permeabilization activity, we plotted the percentage change in NBD F/F_0 against the amount of dye release for a fixed early time point. Dye release values were normalized to that of WT Bax to provide a measure of relative activity. This analysis showed that, following activation by either cBid or Bim, NBD-labelled residues again fell into two classes (Figures 2c and 2d). For residues outside the BH3-binding groove, rates of NBD fluorescence change were correlated with rates of permeabilization, suggesting that kinetic variation within this group reflected differences in overall activity rather than differences in the relative timing of conformational changes. However, residues in the BH3-binding groove (54, 62, 68, and 79) exhibited substantial early changes in fluorescence not attributable to differences in rates of permeabilization, suggesting that these residues, as a group, participate in a local intermediate conformational change preceding pore formation (Figures 2c and 2d).

To analyze the timing of NBD fluorescence changes relative to dye release, we calculated the time derivatives of both curves (shown for Bax-15C-NBD and Bax-54C-NBD in Figure S2a). While the rate of change of NBD fluorescence is almost invariably fastest at the initial timepoints, the rate of change of dye release reaches a maximum before declining to zero at steady state. This process is evident in the dye release time-courses as a slight lag phase at the earliest timepoints and is also observed for wild-type Bax (Appendix Section 1). Strikingly, for Bax-54C-NBD, a BH3-region mutant exhibiting both non-monotone kinetics and a measurable lag phase in dye release, the timepoint at which the maximum NBD fluorescence is reached (the zero of the NBD derivative) corresponds very closely to the timepoint at which dye release achieves its maximum rate (the peak in the dye release derivative; gray vertical line, Figure S2a). One interpretation of this finding is that the rate of dye release is proportional to the abundance of an intermediate species associated with increased hydrophobicity at the Bax BH3 region. We conclude that, for residues both within and outside the BH3 region, NBD fluorescence at the labeled residues undergoes a change that precedes pore formation. This suggests the presence of at least one intermediate conformational state for Bax that exists prior to pore formation

Kinetic modeling reveals three distinct conformational states

To investigate the number of fluorescence transitions in our data, and the degree to which each of the labeled residues participated in these transitions we create a series of ODE-based models. We first considered a simple kinetic model involving linked transitions between conformational states of Bax, each with different level of NBD fluorescence:



The model posits an inactive soluble Bax (Bax_{C0}) state and membrane-inserted pore (Bax_{Cn} ; see Methods) linked via an unknown number of intermediate Bax conformations. The model assumes that the introduction of labels at different positions in Bax may alter transition rates between conformations (as described above) but does not change the total number of conformations. We used Bayesian parameter

estimation to fit models involving 2 to 5 conformations to the kinetic data for each residue (Methods). The kinetic curves for several labelled mutants were well-approximated by a simple two-state model and a corresponding single-exponential equation (Methods). This is most evident for residues outside the BH3-binding groove (e.g. 3 and 126 in Figure 3a). However, the non-monotonic fluorescence curves for labelled residues in the BH3-binding groove (54, 62, 68, and 79) were fit very poorly by the single-exponential two-state model but well by a three-state model (54 in Figure 3a).

To rigorously assess the relative performance of different kinetic models we calculated the marginal likelihood for each model. This approach accounts for uncertainty in rates by integrating the quality of fit across a full range of plausible parameter values (Methods)²⁰. For most residues, but particularly those in the BH3 region (Figure 3b, red points) and α 5-6 (green points) we observed a dramatic improvement in overall fit for a three-conformation model as compared to a two-conformation model (left and right panels in Figure 3a) with a corresponding improvement in model likelihood (Figure 3b). Only a small number of labelled residues had a substantially increased marginal likelihood with the addition of a fourth or fifth conformational state (Figure 3b); in this case, a slight improvement in fit is outweighed by a penalty on increasing model complexity. The improvement in likelihood for the three-conformation model spanned all labeled regions (N-terminus, BH3 region, α 5-6, α 9; Figure 3b) suggesting that the insertion process involves coordinated changes across the protein that can be grouped into three states:



where C_0 is the aqueous conformation, C_2 is a membrane-inserted translocation-competent pore found at equilibrium, and C_1 is a transient intermediate linking the two.

cBid and Bim cause Bax to undergo a rapid transition to an intermediate conformation that precedes pore formation

Bayesian parameter estimation yielded estimates not only for the apparent rate constants (k_1 and k_2) linking Bax conformations, but also for the NBD fluorescence intensities of the intermediate (C_1) and final (C_2) conformations; k_1 , k_2 , C_1 and C_2 values were thereby obtained for each labelled residue. Fluorescence intensities for C_1 and C_2 correlate with hydrophobicity in the local environment of a labelled residue, providing information on protein proximity to the membrane. For 16 of 19 residues examined, the fitted value for k_1 was ≥ 6 -fold higher than k_2 , showing that the transition from the intermediate to final conformation is rate limiting (Figure S2b). Since multiple studies have shown that residue L120 is embedded within the bilayer^{12,21,22} a “burial index” was generated by normalizing all fitted fluorescence values (C_0 , C_1 and C_2) to the fluorescence of fully-buried L120C in the final (C_2) state (Figure 3c). Based on this, a threshold of 50% was set to discriminate qualitatively between residues more or less likely to be buried in the bilayer¹². With the exception of residue 62, residues in the N-terminus (36, 40 and 47) and the BH3-binding groove (54, 68 & 79) were more hydrophobic in the intermediate than in the final state ($C_1 > C_2$; Figures 3c and 3d). The lower burial indices for these residues compared to that of L120C suggests that these residues were not fully inserted in the membrane. Instead, we propose that the increase in burial index of these residues from the C_0 state could result from the formation of a protein-protein interface or interaction with the membrane surface²³. The final burial indices (C_2) of residues in the N-terminus and BH3-binding groove are substantially lower than those of residues in $\alpha 5$ -9 (Figure 3c), consistent with a model in which the BH3-binding groove ($\alpha 2$ -4) is above the membrane or lining the pore^{10,11}.

Labelled residues lying in $\alpha 5$ -6 and $\alpha 9$ exhibited greater burial indices in the C_1 and C_2 states compared to the C_0 state, consistent with their known role in membrane binding and pore formation^{11,12,21}. Several residues (120, 122, 126, 151, 175) had a fitted C_1 value associated with a burial index $> 50\%$, suggesting that they may be partially inserted in the intermediate state. The profile of the final C_2 burial index values across these residues is consistent with key features of current structural models of the assembled Bax pore. In particular, residues 120, 122 and 126, which lie in $\alpha 5$, attained high burial index

values, whereas residue 138 on $\alpha 6$ reaches a level between the aqueous and fully embedded environments (Figure 3c). These data are consistent with insertion of $\alpha 5$ into the lipid bilayer^{11,13}. Residue 151 of alpha $\alpha 7$ has a comparable C_2 burial index to residues 120-126, consistent with different models where $\alpha 6$ is either buried within the bilayer or is partially buried, lying in-plane with the bilayer^{13,22}. Finally, the burial index of residues in the middle of helix 9 (175, 179) are moderately high whereas residues at the end of the helix (184 and 188) are very low, confirming that $\alpha 9$ spans the bilayer with the C-terminus exposed to aqueous solvent^{9,12,21,22,24} (Figure 3c).

Taken together, these data suggest that Bax activation involves a fast transition (k_1) from an initial aqueous conformation (C_0) to a pre-pore intermediate (C_1) involving an increase in local hydrophobicity across most of the protein. This change is a transient one for multiple residues in the BH3-binding groove (Figure 3d). Bax then undergoes a slower transition (k_2) to a final conformation (C_2) in which the membrane-binding helices $\alpha 5$, $\alpha 6$ and $\alpha 9$ move to the highly hydrophobic environment that characterizes a fully inserted Bax pore.

Bim and cBid activate Bax by a similar mechanism

Activating BH3 proteins have the potential to bind to an N-terminal ‘rear’ pocket of Bax, which is composed of $\alpha 1$ and $\alpha 6$, and a canonical ‘front’ BH3-binding groove^{12,25,26}. Both of these interactions serve to displace $\alpha 9$, thereby exposing the BH3-binding groove of Bax. To date, Bim is the only activator BH3 protein reported to bind the Bax ‘rear’ pocket²⁵ whereas both cBid and Bim bind the front BH3-binding groove¹⁰. Given differences in binding mode, we wondered whether cBid and Bim would activate Bax via alternate mechanisms resulting in different Bax conformation states. To investigate this, we compared the hydrophobicity of NBD labelled residues for the C_0 , C_1 and C_2 conformations following exposure to cBid or Bim. We found that the hydrophobicity for each labelled residue in different Bax confirmations were similar for activation by cBid and Bim, as judged by the Pearson correlation coefficient ($r > 0.87$; Figure 4a). However, the rate constants k_1 and k_2 were not well fit by linear regression and were only weakly correlated ($r = 0.27$ for k_1 and -0.032 for k_2 ; Figure 4b). In general, the

rate constants were faster following Bax activation by cBid as compared to Bim (Figure 4b, grey versus black bars). Although cBid and Bim have been reported to interact with Bax differently, from these data we conclude that cBid and Bim cause Bax activation to proceed through the same sequence of conformational states although the rate of the reaction differs by as much as 10-fold (Figure 4b).

The intermediate conformation is associated with binding of activator BH3 proteins to Bax whereas the final conformation is associated with Bax insertion into membranes and pore formation

To investigate protein-protein interactions involved in initial BH3 protein binding to Bax and subsequent Bax oligomerization we combined FRET and NBD fluorescence measurements. FRET between Bax and either cBid, Bim or Bax was measured using those NBD-labeled Bax proteins that had near wild-type activity in pore formation^{15,17} (Figure 5a, left and middle panel; Appendix section 2 and 3). Hypothesizing that the protein-protein interactions measured by FRET would correspond closely in time to the hydrophobicity changes indicated by NBD, we fit the data using an extended three-conformation kinetic model having a single set of rate parameters (k_1 and k_2) and four fluorescence scaling parameters: two parameters for the NBD fluorescence of the intermediate and final states, and two parameters for the FRET between Bax and the interacting partner in the intermediate and final states (Figure 5a; right panel; the FRET scaling parameter associated with the initial state was fixed at zero).

Fluorescence time courses for both FRET and NBD fluorescence were well-fit by this model, showing that intermolecular interactions and local hydrophobicity changes occurred on the same timescales. This can be seen by overlaying the *maximum a posteriori* model fits (that is, kinetic trajectories simulated by using the highest likelihood parameter values) against normalized kinetic traces for FRET (green dots), NBD emission (blue dots) and liposome permeabilization (black dots; Figure 5b). For Bax-54C-NBD, the early peak in NBD fluorescence is coincident with that of Bid-Bax FRET (Figure 5b; top-left panel, blue curve rises with green curve) but precedes the onset of Bax-Bax FRET (Figure 5b;

top-right panel, blue curve left of green curve), suggesting that the Bid-Bax interaction coincides with the transition from C_0 to C_1 . On the other hand, Bax-126C-NBD reaches its maximal NBD fluorescence well after Bid-Bax FRET (Figure 5b; bottom-left panel, green curve left of blue curve) but coinciding with Bax-Bax FRET and liposome permeabilization (Figure 5b; bottom-right panel, blue curve overlaps green curve). Similar results were observed when Bim was used as the activator (Figure S3a). Notably, cBid-Bax and Bim-Bax FRET levels at equilibrium were well above baseline for all residues measured, indicating that at least a subpopulation of Bax remains in close proximity to its activator even after the onset of pore formation (Appendix Section 2).

To consolidate results across all residues in an interpretable way, the normalized initial rates of FRET and NBD emission (computed from the model fits) were adjusted for differing levels of Bax activity by dividing by the FRET and NBD initial rates by the rates of liposome permeabilization on a per-labelled residue basis (Figure 5c, S3b). This enabled ordering of proportional NBD emission change (percentage of maximum) with respect to early steps - BH3 protein interacting with Bax - or late steps - Bax oligomerization and pore-formation. The proportional initial rate of the interaction between cBid and Bax was found to be greater than that of liposome permeabilization for all residues (Figure 5c left panel; cBid:Bax FRET, green bars, versus membrane permeabilization, black bars). Results were similar when Bim was used as the Bax activator (Figure S3b), confirming that BH3-protein binding to Bax is an early event occurring before Bax fully inserts into the membrane. By contrast, the proportional initial rate of Bax oligomerization was similar to that of liposome permeabilization (Figure 5c right panel; Bax:Bax FRET, green bars, versus membrane permeabilization, black bars), confirming that Bax oligomerization is a late event associated with pore formation.

Residues fell into two classes with respect to differences in the normalized initial rates of NBD emission to the rates of either cBid/Bim interaction with Bax or liposome permeabilization (Figure 5c left panel, S3b). Residues 36 and 54 had rates of NBD emission similar to rates of cBid:Bax or Bim:Bax FRET (blue vs. green bars), while the remainder (residues 3, 126, 138 and 175) had rates of

NBD emission similar to rates of membrane permeabilization (blue vs. black bars). When comparing NBD emission to Bax oligomerization, only residue 54 had an initial rate of NBD emission larger than that of Bax oligomerization (Figure 5c right panel, blue vs. green bars), whereas other residues had rates similar to those of Bax oligomerization. These data show that the timescale on which the BH3-binding groove as (represented by Bax-NBD-54C) reaches its maximal change in hydrophobicity is correlated with activator BH3 protein binding to Bax (Figure 5d), a finding that is also consistent with the kinetic traces shown in Figure 5b. The change in the $\alpha 1$ - $\alpha 2$ loop (residue 36) of Bax occurs at an indeterminate time-point between activator BH3 protein binding and Bax oligomerization (Figure 5d). In contrast, maximal hydrophobicity changes in the N-terminus, $\alpha 5$, $\alpha 6$ and $\alpha 9$ (residues 3, 126, 138 and 175 respectively) are associated with Bax oligomerization and Bax pore formation (Figure 5d). We conclude that initial interaction of Bax with an activator BH3 protein results in a global Bax conformational change marked by a transient increase in the local hydrophobicity of the BH3-binding groove; this intermediate conformation corresponds to C_1 and involves binding of Bax to the activator BH3 protein. Bax then undergoes a second conformation change to a final membrane-inserted state (C_2) in which $\alpha 5$, $\alpha 6$ and $\alpha 9$ reach their maximal hydrophobicities, closely associated in time with Bax oligomerization and pore formation. Thus, the three-conformation model of Bax proposed above is sufficient to account for the dynamics of both protein-membrane and protein-protein interactions during the Bax activation process.

Cancer-associated Bax mutants have defects in conformation transitions required for pore formation

Bax acts as a tumour suppressor by inducing apoptosis in cancer cells. Thus, mutations in Bax that disrupt pore formation reduce apoptosis^{27,28}. If our kinetic model is correct, we might expect to identify cancers carrying Bax mutations that prevent acquisition of the active C_2 state that is necessary for membrane permeabilization. To investigate this possibility we compiled from cBioPortal^{29,30} a list of Bax mutations found in human cancer. The most common mutations involve truncations and frameshifts upstream of the BH3-motif (residue E41) which are expected to abrogate all Bax function. Multiple less

frequent missense mutations were also identified throughout the rest of the protein (Figure 6a), of which we selected 15; we also added 4 Bax mutants (G108E, G179E, S184E, S184V) not found in cancer but previously characterized as affecting Bax function *in vitro*³¹⁻³⁵.

We cloned, expressed and purified 19 Bax mutations and tested their liposome permeabilization activity (Figure 6b). Six of these (G67R, G108E, G108V, L113P, G179E, and S184E) were 2- to 30-fold less active than wild type. These mutants were labeled with NBD at C126 and their interaction with cBid, insertion of α 5-helix into membranes, and pore formation were characterized by FRET with cBid, 126C-NBD emission and liposome dye release (Figure 6c). The L113P mutant did not interact with cBid, insert into the bilayer or form pores; it was therefore blocked at C_0 . G179E interacted with cBid and permeabilized liposomes, but appeared to have an altered C_2 state with an EC_{50} for membrane permeabilization (Figure 6b) roughly twice that of WT Bax. G179E also had a relatively low level of α 5-helix insertion, consistent with a defect in pore formation (Figure 6c).

The other mutants G67R, G108V, G108E and S184E represented proteins that appeared to be blocked at the C_1 conformation. They interacted with cBid but had low levels of α 5-helix insertion and pore formation. To demonstrate this we labelled G67R, G108V and S184E Bax at position 54C using NBD and then collected fluorescence time-course data following activation with cBid (we were unable to achieve efficient labeling of residue 54C in the G108E mutant). The Bax 54C-NBD fluorescence emission time course is a useful measure of the C_1 to C_2 transition since fluorescence initially rises with C_1 and then falls with C_2 (Figure 5b; residue 54C). Both the G67R and S184E mutants exhibited high levels of FRET between cBid and the 54C-NBD label (Figure 6d, green bars) as well as high and sustained NBD fluorescence (as compared to WT Bax labelled with NBD at residue 54C; Figure 6d, blue bars). This shows that G67R and S184E Bax are able to interact with cBid and but they are not able to complete the activation process (Figure 2b, 5b), consistent with a block in C_1 , further confirming the existence of this intermediate state.

The G108V mutant exhibited high level of FRET with cBid when the NBD label was on Bax residue 126C (Figure 6c, green bar) but much less FRET with cBid when the NBD label was on Bax residue 54C (Figure 6d, green bar) perhaps because (i) addition of two mutations to the Bax BH3-binding groove (54C-NBD and G108V) alters Bax such that it no longer interacts with cBid, or (ii) the NBD fluorophore at position 54C is not properly aligned for FRET with the DAC fluorophore on cBid when Bax also has the G108V mutation. We reason that the latter explanation was more likely since there we generally observe increased NBD emission from residue 54C-NBD upon BH3 protein binding and a small amount of FRET was detected.

The Bax point mutants G67R, G108V and S184E all had increased fluorescence emission of NBD at position 54C compared to WT Bax (labelled with NBD at residue 54C) at the timecourse endpoint (Figure 6d, blue bars). This suggests that they do not complete the activation process, which for Bax-54C-NBD corresponds to a decline in NBD fluorescence from an initial peak (Figure 2b, 5b). Indeed, the kinetics of NBD emission at position 54C for the Bax point mutants G67R, G108V and S184E revealed that these mutants only increase in fluorescence emission (Figure 6e), as would be expected if these mutants trap Bax in the intermediate conformation.

From these data, we conclude that point mutations in Bax can affect the process of pore formation at all three steps, with some mutations preventing the initial transition to a required intermediate conformation (L113P), and others the transition from this intermediate to inserted in membranes (G67R, G108V, G108E, S184E) and finally one mutant with a defect in Bax oligomerization or pore formation (G179E).

Discussion

By combining multiple time-resolved assays of Bax conformation, Bax interaction with cBid or Bim, and formation of functional pores in a reconstituted system we have resolved several outstanding questions about the mechanism of Bax activation. Kinetic modeling using ODEs played an important role

in our analysis because it allowed the likelihood of different kinetic schemes to be evaluated against complex and heterogeneous data. For example, in the case of Bax proteins labelled at different sites with NBD, modeling made it possible to untangle the impact of conformation on fluorescence intensity (the data we were seeking) from the inhibitory effects of labelling on Bax activity (a confounding factor). In addition, by comparing model-based predictions to all available fluorescence and FRET data, it was possible to demonstrate that our final model is maximally consistent with experimental evidence. Based on this reasoning we conclude that activation of Bax by BH3 proteins involves transitions between three distinct Bax conformations: a soluble monomer (C_0), a membrane-associated pre-pore intermediate that is bound to activator BH3 proteins (C_1) and a final pore-forming conformation (C_2). The transition from initial (C_0) to the intermediate (C_1) conformation is faster than the transition from the intermediate (C_1) to the final (C_2) state (Figure 7).

Our three-state model clarifies data found in several previous publications. For example, we have shown that while the Bim BH3 motif is absolutely required to activate Bax, the carboxy-terminal sequence of Bim also interacts with Bax to aid in Bax activation, implying that Bim interacts with Bax differently than cBid, which lacks the C-terminal motif.³⁶ However, the data in this paper show that cBid and Bim activate Bax via the same sequence of conformational changes (Figure 4). Thus, regardless of exactly how cBid and Bim interact with Bax, with respect to Bax the activation pathway is the same. Additionally, it is puzzling that cBid and Bim engage the BH3-binding groove of Bax during activation^{10,26}, but binding of this groove by the BH3-motif of another Bax molecule is necessary for oligomerization and pore formation^{10,37,38}. Furthermore, addition of activator BH3 in excess to Bax does not inhibit pore formation, showing that the Bax BH3-motif and the activating BH3 motifs in cBid and Bim do not directly compete with each other. It therefore seems likely that the BH3-binding groove in Bax changes conformation to preferentially bind to BH3-motifs on Bax monomers rather than to cBid and Bim³⁹. This may be the “function” of the intermediate conformation we have identified in our study. We postulate that rearrangement of the BH3-binding groove in Bax increases the affinity between monomeric

Bax molecules in the intermediate (C_1) conformation such that Bax (C_1) monomers can then form dimer units in the bilayer that oligomerize to form a pore^{2,39}. In this context, it is noteworthy that cBid and Bim continue to exhibit FRET with Bax at equilibrium (Figure 5b, Figure S3a, Appendix Section 2). We propose that cBid and Bim remain bound to Bax even after pores are formed, either via another protein interface, the presence of a sub-population of Bax monomers in C_1 , or conformational flexibility in the C_2 state.

Kinetic studies of Bax conformations during the transition from a soluble monomer to a membrane embedded oligomer provide an interpretive framework for previous data on Bax membrane topology^{12,21,22} and structural studies^{10,26,41}. The burial indices of Bax (Figure 3c) support a model in which Bax is activated in two stages, with the initial transition marked by a temporary increase in the hydrophobicity of the BH3-binding groove of Bax concomitant with binding of activator BH3 motifs. As described above, the initial change in hydrophobicity may result from the BH3-motif of the activator protein triggering changes in the structure of the Bax BH3-binding groove required for Bax to form dimers^{12,42,43}. Only after this initial conformational change do helices α_5 , α_6 and α_9 (green and blue in Figure 7) fully insert into the membrane with the rest of Bax (α_1 -4) remaining in a more hydrophilic environment. This existence of an intermediate state is also consistent with previously published models in which the BH3-motif first interacts with the BH3-binding groove to initiate the formation of Bax dimers via reciprocal BH3-motif and BH3-binding groove interactions between two Bax monomers. Since Bax helices 5 and 6 are both amphipathic it is possible that one side of both helix 5 and 6 is embedded within the bilayer while the other is exposed to solution^{11,22}. Our kinetic analysis suggests that α_5 , α_6 and α_9 insert into the bilayer simultaneously while Bax undergoes significant structural rearrangements across the entire protein. This data appears to contradict current models in which Bax first inserts α_9 into the bilayer, thereby adopting a tail-anchored topology before BH3 proteins bind Bax^{10,44,45}. Our explanation for this discrepancy is that previous results were obtained using Bax mutated in α_9

residues and/or subjected to crosslinking. We speculate that the tail-anchored topology is possible only under these circumstances.

The existence of point mutations (e.g., G67R, G108V, and S184E) that block Bax activation in a membrane-bound but nonfunctional state having properties similar to those of the C₁ intermediate confirms a requirement for C₁ in pore formation. Because membrane insertion of Bax is the rate-limiting step in apoptosis (Figure S2a)^{15,39} it is not unreasonable that such mutations would also be found in human tumors. Such mutant Bax proteins are expected to sequester activator BH3 proteins and act in a dominant negative manner. Consistent with this, we recently discovered that Bax S184E is dominant to WT Bax in preventing liposome permeabilization in reconstituted systems and apoptosis in cells following exposure to a range apoptotic stimuli³⁵.

There exists substantial interest in developing therapeutic inhibitors of Bax and Bak as a means to prevent pathologic cell death. Such inhibitors might work in circumstances in which inhibition of executioner caspases alone is insufficient to block cell death following MOMP^{46,47}. The dual nature of the BH3-binding groove of Bax as both a site of activation and dimerization suggests that it will be necessary to identify chemical ligands that act as inhibitors and not agonists against a single binding groove. In particular, the BH3 binding pocket of the C₁ intermediate conformation may be a good target for an inhibitor, since binding is expected to prevent the subsequent steps of Bax insertion into membranes, dimerization and pore formation. Since the intermediate conformation is kinetically distinct, and transition out of this state to a membrane-inserted Bax is rate-limiting, we predict that the C₁ to C₂ transition also blocked by small molecules acting allosterically⁴⁸.

Recently Brouwer *et al* engineered a Bim-BH3 peptide containing non-natural amino acids that had sufficiently high affinity for the BH3-binding groove to inhibit Bak activation⁴⁹. This occurred because the engineered peptide had slower on and off rates for the Bak BH3-binding groove than the WT Bim-BH3 peptide. Thus, binding and unbinding by activator BH3 proteins may be necessary in order to

accommodate Bax dimerization via reciprocal binding of the BH3-binding grooves between two Bax molecules. These data suggest that small molecules or peptides that bind to the Bax BH3-binding groove can be engineered to either activate Bax by having fast on and off rates or inhibit Bax by stabilizing the intermediate conformation. The methodology described in this paper could be used to identify such molecules^{47,48,50,51}. More generally, the combination of dynamic measurement and dynamic modeling described here may provide an approach to mechanistic analysis of other multi-state, multi-compartment biological reactions.

Figure Captions

Figure 1: Assaying dye release and conformational changes of labelled Bax mutants.

- a. Bax is proposed to adopt many different conformations during activation. All models agree that that in dividing cells Bax exists as a soluble cytoplasmic monomer (conformation **I**) that transitions to the bilayer, oligomerizes (**V**) and forms a pore (**VI**) as a result of activation by a BH3 protein. However, the mechanism of Bax activation remains uncertain with respect to the number and order of Bax conformation changes, and where BH3 proteins are required in the activation mechanism. Current models propose multiple Bax conformations (**I** to **VI**) and transitions (solid arrows) between the conformations where activator BH3 proteins bind to and activate Bax (dotted arrows). The BH3 protein, Bim is proposed to bind to Bax in solution (**I**) at the rear pocket resulting in the exposure of Bax BH3 motif and $\alpha 9$ (**II**), Bax then transitions to the membrane by insertion of *only* $\alpha 9$ into the bilayer and adopting a tail-anchored topology (**IV**) where Bim can then bind the canonical BH3-binding groove causing Bax $\alpha 5$, $\alpha 6$ to insert partially or fully into the membrane bilayer resulting in Bax oligomerization (**V**) and pore formation (**VI**)⁴⁴. Other models propose that Bax first inserts a $\alpha 9$ into the bilayer (**III**) either spontaneously or in response to BH3 protein binding to the canonical groove of soluble Bax (**I**), which displaces $\alpha 9$ from the BH3-binding groove^{10,52,53}. If spontaneously, BH3 proteins can then engage the BH3-binding groove of Bax (**III**) resulting in exposure of the BH3 motif (**IV**). Binding of BH3

proteins to the BH3-binding groove of either Bax (III) or Bax (IV) results in partial or full insertion of Bax $\alpha 5$ and $\alpha 6$ into the bilayer where Bax forms domain-swapped dimers (V) that oligomerize and form pores (VI).

- b. Top: Linear representation of Bax with positions of engineered cysteine mutations used for NBD labeling. The regions of Bax known to undergo conformation changes are highlighted with the corresponding amino acids or helices that make up each region located below: $\alpha 1$ - $\alpha 2$ loop (35 – 53), BH3-binding groove (54 – 99), BH3 motif (63 – 71), and membrane inserting helices ($\alpha 5$, $\alpha 6$, $\alpha 9$). Bottom: Solution structure of Bax (PDB ID: 1F16) with positions of engineered cysteine mutations used for NBD labeling marked in red.
- c. Schematic of the multiplexed fluorescence spectroscopy assay. An activator BH3 protein such as cBid is added to liposomes that contain the fluorescent complex of Tb:DPA (terbium:dipicolinic acid) and allowed to equilibrate. In liposomes Bim is faster than cBid at recruiting Bax to membranes because cBid undergoes a conformational change within the membrane before Bax is recruited^{19,54}. Therefore, the activator proteins were pre-incubated with liposomes for 5 minutes before Bax was added to ensure the conformational changes and membrane binding had come to equilibrium. This allowed comparable ordering of Bax conformation changes because the different kinetics of the activator BH3 proteins are not included in the subsequent analysis. NBD-labelled Bax mutants are then added and fluorescence time courses are recorded. Pore formation is measured as a decrease in Tb:DPA fluorescence (black line) as it is released into the solution, which contains EDTA that rapidly chelates Tb, thereby dismantling the Tb:DPA complex. Bax conformational changes and membrane interactions are indicated by the fluorescence changes of NBD-Bax (blue line).

Figure 2: Kinetics of NBD fluorescence changes.

- a. One hour endpoint of the relative change of NBD emission (F/F_0) at 530 nM of 100 nM Bax labelled at the indicated residue after the addition of 20 nM cBid (grey) or 20 nM Bim (black) in

the presence of Tb:DPA encapsulated liposomes. Shown is the average of 3 independent experiments each with one technical replicate. Error bars represent the standard deviation ($n=3$).

- b.** Example NBD-Bax fluorescence time courses of the relative change of NBD emission (F/F_0) at 530 nM after the addition of cBid. Each of the eight time courses shown is one of three replicates where 20 nM cBid and 100 nM Bax labelled with NBD at the indicated residue were incubated together in the presence of Tb:DPA encapsulated liposomes.
- c.** , **d.** Percentage of maximum NBD F/F_0 change plotted against dye release relative to WT Bax at a fixed early time-point (105 sec), using cBid as the activator. Shown is the average of 3 independent experiments each with one technical replicate. Error bars represent the standard deviation ($n=3$). Data from non BH3 residues (N-terminus, $\alpha 5-6$, $\alpha 9$) was fit to a straight line. **d.** Same as Figure 2c (above) but using Bim as the activator.

Figure 3: Fits of kinetic models to NBD fluorescence time courses.

- a.** Fits of a two-conformation (left panels; red line) or three-conformation (right panels; blue line) model to Bax 3C-NBD, 54C-NBD and 126C-NBD fluorescence emission (F/F_0) time course data (black points). Data shown is representative of a single replicate of Bax activated with cBid.
- b.** Marginal likelihood values calculated for different models for all NBD time course replicates in the dataset by Markov chain Monte Carlo sampling (Methods). Lower $-\ln(\text{Marginal Likelihood})$ values for a specific model indicate improved fit to data across a wide range of parameter values and hence increased support. Each NBD time course replicate is colour-coded based on where NBD is labelled on Bax (purple: N-terminus; red: BH3-binding groove; green: $\alpha 5, \alpha 6$; blue: $\alpha 9$). Inset shows differences between the three, four, and five conformation models on an increased scale. Boxes extend from the first to the third quartile of the data, with a horizontal line at the median; whiskers extend above and below to $1.5 \times$ the interquartile range.

- c. Maximum a posteriori (MAP) values (point estimates) of the absolute fluorescence in C_0 , C_1 and C_2 were calculated from the fit of the three-conformation model to each replicate. A residue burial index was generated by normalizing the MAP values to the average MAP value (across replicates) of the predicted fluorescence of Bax L120C-NBD in the final conformation (C_2). Shown is the average and standard deviation of the MAP values for 3 independent replicates, each with one technical replicate ($n=3$).
- d. Schematic interpretation of the results from fitting the NBD and terbium time-course data to the three-conformation model. Bax undergoes a fast (k_1) transition from an initial inactive hydrophilic conformation (C_0) to an intermediate conformation (C_1) marked by a transient increase in the hydrophobicity of the BH3-binding groove. Bax then undergoes a second slower (k_2) transition into a final conformation (C_2) that is associated with the insertion of Bax into the bilayer.

Figure 4: Bid and Bim activate Bax via similar mechanisms

- a. Comparison of C_0 (left), C_1 (middle) and C_2 (right) parameters for different Bax residues labelled with NBD and activated by cBid (grey) or Bim (black). Shown is the average of C_0 , C_1 and C_2 parameters divided by 1000 and represented as arbitrary units (A.U.). C_0 values are the absolute fluorescence values from the fluorimeter for each residue. C_1 and C_2 are the maximum a posteriori (MAP) values (point estimates) of the absolute fluorescence predicted from fitting the NBD time-course data for each of the indicated residues of NBD labelled Bax to the 3 conformation model. Below each bar plot is a scatter plot comparison of the C_0 , C_1 and C_2 MAP values for each independent replicate (coloured dots) for each Bax residue located in the bar plots above ($n=3$) where all replicates for all residues were fit to a straight line (solid black line) with 95% confidence intervals (black dotted line). Pearson's correlation coefficients were calculated for each comparison of Bid versus Bim C_0 , C_1 and C_2 values where a coefficient of 1 means perfect

correlation between values, a coefficient of 0 means no correlation between values and a coefficient of -1 means perfect negative correlation between values.

- b. MAP values of k_1 (left) and k_2 (right) parameters, plotted as for C_1 and C_2 in Figure 4a.

Figure 5 – The intermediate (C_1) conformation is associated with a BH3:Bax heterodimer and the final (C_2) conformation is associated with Bax oligomers.

- a. Schematic of multiplexed fluorescence spectroscopy assays fit with linked kinetic parameters.

Left: An activator BH3 protein (cBid or Bim) and NBD-labelled Bax are incubated with Tb:DPA encapsulated liposomes and liposome permeabilization (Tb:DPA release; black) and conformation change (NBD emission; blue) are tracked. In addition, protein-protein interactions (FRET; blue) are tracked using three separate assays. 1) cBid-DAC was used to measure the interaction between cBid and Bax-NBD, 2) Bim-DAC was used to measure the interaction between Bim and Bax-NBD, and 3) Bax-DAC was used to measure the interaction between Bax proteins (Bax oligomerization). *Middle:* In the assays with DAC-labelled cBid or Bim, the activator BH3 protein was added to liposomes and allowed to equilibrate for 5 minutes followed by the addition of Bax-NBD. In the assay where DAC labelled Bax was used, unlabelled cBid was added to liposomes and allowed to equilibrate for 5 minutes, followed by the addition of 10 nM DAC labelled Bax and then the subsequent addition of Bax-NBD. Pore formation is measured as a decrease in Tb:DPA fluorescence (black line) as it is released into the solution, which contains EDTA that rapidly chelates Tb, thereby dismantling the Tb:DPA complex. Bax conformational changes and membrane interactions are indicated by the fluorescence changes of NBD-Bax (blue line). Interactions between Bax and activator BH3 proteins are observed by the decrease in fluorescence of the DAC-labelled activator BH3 proteins due to FRET with NBD-Bax (green line). *Right:* The NBD and FRET time course data was fit to a three-conformation model where fluorescence scaling parameters for NBD emission and FRET percentage were fit independently while a single set of shared rate parameters (k_1 and k_2) were used for both.

b. ,c. and d. NBD labelled Bax residues corresponding to distinct regions of Bax known to undergo conformational changes were assayed in multiplexed fluorescence assays: Bax-3C-NBD (N-terminus), Bax-36C-NBD (α 1- α 2 loop), Bax-54C-NBD (BH3-binding groove), Bax-126C-NBD (α 5), Bax-138C-NBD (α 6) and Bax-175C-NBD (α 9). For each labelled residue separate assays were performed in triplicate for each of the six NBD-labelled Bax variants for a total of 54 assays each contemporaneously tracking liposome permeabilization, NBD emission and protein interactions via FRET between either Bid-DAC and Bax-NBD or Bax-DAC and Bax-NBD. Incubation of NBD-labelled Bax with either DAC-labelled cBid, Bim or Bax resulted in similar extents of NBD emission confirming that the addition of the DAC label does not alter the activation mechanism of NBD labelled Bax (Figure S3c) **b.** Shown is the experimental time course data for liposome permeabilization (black dots), NBD emission (blue dots) and FRET (green dots) of one experimental replicate of assays containing Bax-54C-NBD (BH3-binding groove; top graphs) and Bax-126C-NBD (α 5; bottom graphs). The NBD emission and FRET curves were fit (NBD: blue line; FRET: green line) to the three conformation model (with linked rate parameters, k_1 and k_2 , between NBD and FRET time courses) and maximum a posteriori fits were plotted along with the experimental data. **c.** The normalized initial rate (slope of first 5 data points divided by maximum signal during the full timecourse) was calculated for liposome permeabilization (black), NBD emission (blue) and FRET (green), either between Bax-NBD and cBid-DAC (left) or Bax-NBD and Bax-DAC (right) for each NBD labelled Bax residue assayed. Initial rates of NBD and FRET change are further normalized to the initial rate of liposome permeabilization which allows equal comparison of FRET and NBD emission rates independent of the liposome permeabilization activity of each Bax mutant. Each bar represents the average of 3 independent experiments each with one technical replicate. Error bars represent the standard deviation (n=3). **d.** A judgment was made based on the experimental data and fits to the three-conformation model to place the NBD emission change of each residue somewhere along the Bax

activation pathway using the FRET between activator and Bax, FRET between Bax and Bax and liposome permeabilization as markers for each Bax activation step.

Figure 6: Mechanistic characterization of Bax point mutations in cancer.

- a. Genomic alterations in Bax identified by cancer genome sequencing where the y-axis represents the number of mutations found across all cancers and the x-axis represents which residue in Bax was altered. Data was gathered from cBioPortal and the figure was generated using the cBioPortal data-browsing interface.
- b. Liposome permeabilization activity of Bax point mutants represented by EC_{50} . For these experiments liposomes were incubated with 20 nM cBid and Bax was titrated from 0 to 200 nM and liposome release was measured at a two hour endpoint. The liposome permeabilization data at each concentration of Bax was then fit to an agonist versus response curve and EC_{50} values were calculated. Data shown is the average of 3 independent experiments each with one technical replicate. Error bars represent the standard deviation (n=3)
- c. Endpoint cBid-Bax FRET (green), Bax-C126-NBD fluorescence (blue) and dye release (black) normalized to the values of 'WT' Bax and cBid (Bax-C126-NBD + cBid-DAC) of labelled Bax point mutations. Shown is the average of 3 independent experiments each with one technical replicate. Error bars represent the standard deviation (n=3).
- d. Endpoint cBid-Bax FRET (green), Bax-54C-NBD fluorescence (blue) and endpoint dye release (black) normalized to the values of 'WT' Bax and cBid (Bax-54C-NBD + cBid-DAC) of labelled Bax point mutations. Shown is the average of 3 independent experiments each with one technical replicate. Error bars represent the standard deviation (n=3).
- e. Representative NBD emission time course data of one individual replicate of 100 nM Bax-54C-NBD activated by 20 nM cBid for WT Bax and Bax with either a G67R, G108V or S184E point mutation.

Figure 7: A redefined Bax activation pathway

The current kinetic model of Bax activation suggests that Bax exists as a cytosolic monomer that reversibly tethers to the membrane via helix 9^{10,44,52,53}. Bax is then activated by a BH3 protein from the cytosol in a hit-and-run manner resulting in Bax insertion, oligomerization and pore formation. We find instead that Bax exists in an inactive initial conformation (C_0) as a cytosolic monomer. Membrane embedded activator BH3 proteins, such as tBid, must be present at the membrane in order to recruit and activate Bax. Activator BH3 binding to Bax, does not occur in a hit-and-run fashion and represents a time-resolved Bax:activator BH3 intermediate. This binding facilitates a rapid conformation change in the BH3-binding groove of Bax associated with an increase in hydrophobicity of this region. The intermediate conformation (C_1) of Bax is not fully inserted into the membrane with α -helices 5, 6 and 9 only having slight increases in hydrophobicity. Bax then transitions to a final membrane-embedded conformation (C_2) where helices 5, 6 and 9 insert simultaneously. Insertion of these helices does not appear to occur in a step-wise fashion and is the rate-limiting step in the Bax activation pathway. Upon insertion Bax rapidly oligomerizes forming pores in membranes. Furthermore our data suggests that all potential inserted forms of Bax (monomers, dimers, oligomers and pore-Bax) have similar conformations.

Supplementary Figures

Figure S1

- a. Labelled single-cysteine Bax mutants have been used successfully in several previous equilibrium^{11-13,21,22}, and kinetic^{15,16} structural studies of Bax. Consequently we expected that for most residues in Bax, cysteine substitution and addition of the low-molecular-weight NBD would minimally affect the activity of the proteins. Shown is the one hour endpoint of the percent liposome permeabilization, measured by a decrease in Tb:DPA emission, of 100 nM Bax labelled at the indicated residue after the addition of 20 nM cBid (grey) or 20 nM Bim (black) in the presence of Tb:DPA encapsulated liposomes. Each bar represents the average of 3 independent

experiments each with one technical replicate. Error bars represent the standard deviation ($n=3$). At end-point two-thirds of the labelled proteins were 80-100% as active as unlabelled native protein. However, mutants with NBD-labelled cysteine at positions 40, 68, 79, 120, 179 and 188 have attenuated pore-forming function but still permeabilized at least 40% of the liposomes in one hour, suggesting that the mechanism of permeabilization is unlikely to have been changed significantly.

- b.** Example of the variability in liposome permeabilization timecourses of Bax labelled with NBD at the indicated residues (3, 47, 54, 62, 68, 79, 120, 126). Each of the eight time courses shown is one of three replicates where 20 nM cBid and 100 nM Bax labelled with NBD at the indicated residue were incubated together in the presence of Tb:DPA encapsulated liposomes.

Figure S2

- a.** Maximum a posteriori (MAP) values (point estimates) for the rate parameters defining the transitions from C_0 to C_1 (k_1) and C_1 to C_2 (k_2), for each NBD-labelled Bax mutant. Shown is the average and standard deviation of the MAP values for 3 independent replicates each with one technical replicate ($n=3$).
- b.** Derivatives of NBD (blue) and terbium release (black) time courses for Bax-15C-NBD (left) and Bax-54C-NBD (right) normalized to the maximum rate of change. Derivatives were calculated numerically after processing the curves with a low-pass filter to reduce noise. The curves shown were for the first experimental replicate with cBid as the activator. The vertical grey line is drawn at the peak rate of change of terbium release.

Figure S3

- a.** And **b.**) NBD labelled Bax residues corresponding to distinct regions of Bax known to undergo conformational changes were assayed in multiplexed fluorescence assays: For each labelled residue separate assays were performed contemporaneously tracking liposome permeabilization,

NBD emission and protein interactions via FRET between Bim-DAC and Bax-NBD. **a.** Shown is the experimental time course data for liposome permeabilization (black dots), NBD emission (blue dots) and FRET (green dots) of one experimental replicate of assays containing Bax-54C-NBD (BH3-binding groove; top graphs) and Bax-126C-NBD ($\alpha 5$; bottom graphs). The NBD emission and FRET curves were fit (NBD – blue line; FRET – green line) to the three conformation model (with linked rate parameters, k_1 and k_2 , between NBD and FRET time courses) and plotted overtop the experimental data. **b.** The initial rate (slope of first 5 data points) was calculated for liposome permeabilization (black), NBD emission (blue) and FRET (green) between Bax-NBD and Bim-DAC for each NBD labelled Bax residue assayed. Shown is the initial rate normalized to the initial rate of liposome permeabilization which allows equal comparison of FRET and NBD emission rates independent of the liposome permeabilization activity of each Bax mutant. Each bar represents the average of 3 independent experiments each with one technical replicate.

c. The final NBD emission F/F_0 values for Bax-3C-NBD (N-terminus), Bax-36C-NBD ($\alpha 1$ - $\alpha 2$ loop), Bax-54C-NBD (BH3-binding groove), Bax-126C-NBD ($\alpha 5$), Bax-138C-NBD ($\alpha 6$) and Bax-175C-NBD ($\alpha 9$) are compared between each multiplexed fluorescence assay kinetic dataset (KD) where: KD1) unlabelled cBid was used to activate Bax and no FRET was tracked (dataset shown in Figure 3), KD2) cBid-DAC was used to activate Bax and Bid:Bax FRET was tracked (dataset shown in figure 5) and KD3) unlabelled cBid was used to activate Bax and FRET was tracked between Bax-NBD and Bax-DAC (dataset shown in figure 5). Shown is the average of 3 independent experiments each with one technical replicate. Error bars represent the standard deviation ($n=3$).

Materials and Methods

The accompanying raw dataset, including corresponding dye release, Bax insertion, and FRET time courses between Bax and activators cBid and Bim, is provided in a variety of formats along with source code at (https://github.com/johnbachman/bax_insertion_paper) to facilitate further analyses and hypothesis testing. Plots of raw and processed data can be accessed in the Appendix.

Mutagenesis, purification and labeling of recombinant proteins

Bax, cBid and Bim single cysteine mutants were created via site-directed mutagenesis.

Purification and labeling of Bax, cBid and Bim single cysteine mutants was performed as previously^{17,54}. Site-specific labeling with a cysteine-reactive NBD was accomplished by mutating the two endogenous cysteines of Bax (C62 & C126) to alanine and then introducing single cysteine substitutions along the length of the protein. NBD labeling efficiency averaged ~75% with a range of 56 to 92% (Appendix section 4).

Generation of liposomes

Mitochondria-like liposomes were generated as previously described¹⁷. Briefly, 1 mg lipid film was hydrated with 1 ml assay buffer (200 mM KCl, 10 mM HEPES pH 7.0, 1 mM MgCl₂) supplemented with 1 mM TbCl₃ and 3 mM Dipicolinic acid. This lipid suspension was frozen and thawed 10 times, followed by 10 passes through a 100 nm pore-size membrane. The liposomes were then passed over a 10 mL CL2B gel-filtration column in order to remove unencapsulated Tb:DPA complex.

Fluorescence measurements

Fluorescence measurements were collected similar to that as previously described¹⁵. Fluorescence measurements were made in 1 mL total volume quartz cuvettes using a PTI (Photon Technologies International) fluorimeter. Samples were temperature controlled to 37°C and had constant stirring. The fluorimeter was set to read each fluorescence channel in succession using 5 nm excitation and emission bandwidths with a 1 s integration time. Channel reads were in the following order: 1) Tb:DPA fluorescence (290 excitation nm, 490 emission nm), 2) DAC Fluorescence (380 nm excitation, 460 nm emission) and 3) NBD fluorescence (475 nm excitation, 530 emission).

Background measurements were collected from sample cuvettes containing 250 μ l of Tb:DPA encapsulated liposomes and 750 μ l of Assay buffer supplemented with 5 mM EDTA in order to quench released Tb:DPA. Background was measured for 300s before the addition of 20 nM cBid or 20 nM Bim (labelled or unlabelled depending on the experiment). In liposomes Bim is faster than cBid at recruiting Bax to membranes because cBid undergoes a conformational change within the membrane before Bax is recruited^{19,54}. Therefore, the activator proteins were pre-incubated with liposomes for 500 seconds before Bax was added to ensure the conformational changes and membrane binding of the activators had come to equilibrium. After reading for 500s 100 nM of NBD labelled single cysteine mutants of Bax was added. Fluorescence was measured for another 3600 s before the addition of 0.5% w/v CHAPS to lyse the liposomes.

% Release was calculated as:

$$\% \text{ Release} = 100 * \left(1 - \frac{F_f - F_{chaps}}{F_i - F_{chaps}}\right)$$

Where F_i was the fluorescence before addition of 100 nM Bax, F_f was the fluorescence before the addition of CHAPS and F_{chaps} was the fluorescence after the addition of CHAPS

FRET efficiency was calculated as:

$$\% \text{ FRET Efficiency} = 100 * \left(1 - \frac{F_{DA} - F_{bg}}{F_D - F_{bg}}\right)$$

Where F_{DA} is the fluorescence DAC in a sample containing both the DAC labelled donor and NBD labelled acceptor, F_D is the fluorescence of DAC in a channel containing both the DAC labelled donor and an unlabelled acceptor, F_{bg} is the fluorescence before the addition of DAC labelled protein. The DA and D only samples were measured in parallel using a turret which rotates samples into and out of the excitation light.

NBD F/F0 was calculated as:

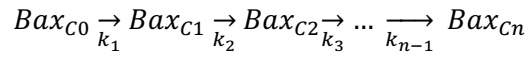
$$\frac{F}{F_0} = \frac{F - F_{bg}}{F_0 - F_{bg}}$$

Where F is the fluorescence of the NBD channel after the addition of Bax, F_0 is the first fluorescent measurement upon the addition of NBD labelled protein and F_{bg} is the measurement of the NBD channel before NBD labelled protein was added to the sample. For several FRET experiments we observed transient but extreme fluorescence values; we believe these to be due to fluorescent debris in the solution and therefore removed these outliers manually in a preprocessing step.

For detection of cBid or Bim interaction with Bax, single cysteine mutants of cBid and Bim were created in which the cysteine was located 1 residue N-terminal of the H0 residue in the BH3-motif of cBid and Bim (residues 85 and 89 respectively) as these residues should be in close proximity to Bax during binding¹⁰.

Kinetic modeling and simulation

We model Bax conformational changes as a set of irreversible transitions between a set of discrete conformational states:



Observed fluorescence at time t was assumed to be the sum of the fluorescence of different conformers weighted by their concentrations:

$$NBD(t) = \sum_{i=1}^n C_i [Bax_{Fi}(t)], \quad (2)$$

where C_i denotes the NBD fluorescence of each of the i conformations of Bax. This model is a simplified version of the generalized scheme involving both forward and reverse transitions, with no loss of generality in terms of its ability to identify the number of conformational states since both formulations are reducible to a sum of n exponential functions. In addition, experimental evidence indicates that the net

off-rate between membrane-bound and aqueous Bax is approximately an order of magnitude slower than the timescale of our experiments⁵⁵.

The irreversible transition model with n states has $n-1$ fluorescence transitions and $2n-2$ free parameters: $n-1$ transition rate parameters and $n-1$ fluorescence scaling parameters; the fluorescence associated with the initial aqueous state of Bax, Bax_{F1} , can be calculated directly from the data. A Gaussian-distributed error model for fluorescence data based was included to make it possible to estimate goodness of fit in light of experimental uncertainty.

Kinetic models were built programmatically using PySB⁵⁶. The models were formulated as sets of mass action ordinary differential equations and simulated either by 1) numerical integration using the VODE integrator⁵⁷ accessed via the Scipy library in Python⁵⁸ or 2) solved directly using a closed-form, analytical solution for the system.

Parameter estimation and model discrimination

Parameter estimation and model discrimination were performed using affine-invariant Markov chain Monte Carlo (MCMC) sampling implemented by the Python software package emcee⁵⁹ and based on the algorithm described by Goodman and Weare⁶⁰. Parallel tempering was used to aid convergence and to calculate marginal likelihood values by thermodynamic integration^{61,62}. For each MCMC run, a ladder of 50 different temperatures was used, with 400 walkers at each temperature. Values for the reciprocal temperature, $\beta = 1/T$, were spaced logarithmically from 1 to a maximum temperature of $\beta = 10^{-6}$. Starting positions for the walkers were chosen randomly from the prior distributions for each parameter. Uniform prior distributions for the kinetic parameters bounded by the relevant timescales of the experiment (10^{-1} to 10^{-6} sec^{-1}) were chosen for analysis. Two prior probability distributions for fluorescence scaling parameters were considered based on the relative and absolute dynamic ranges for NBD: one uniformly distributed and the other Gaussian with greater probability assigned to smaller relative changes. The

results were similar for both but the latter is more plausible as none of the residues exhibited a fluorescence increase greater than 5-fold over baseline.

Convergence of the MCMC chains was assessed by several heuristics: 1) the log marginal likelihood ($\log(\text{ML})$) values were calculated by thermodynamic integration every 50 steps and assessed for asymptotic convergence by comparing $\log(\text{ML})$ from the last 50 steps to the $\log(\text{ML})$ value calculated from the previous 50 steps. If the difference in $\log(\text{ML})$ was greater than an absolute threshold of 3, or greater than a relative threshold of $0.1 \times \text{err}$, where *err* was the error associated with the thermodynamic integration procedure itself, then the chain was considered to be non-convergent. 2) If the chain passed the test of convergence described in (1), the chains at each of the 50 temperatures were assessed for any trend towards increases in posterior probability over the 50-step convergence interval by performing linear regression on the posterior probability values associated with the sampled positions. If the trend for any of the 50 chains was positive with *p*-value less than 0.001, the chain ensemble was considered to be non-convergent. If a chain passed the programmatic heuristics in 1) and 2), the “burn-in” period was terminated and samples were recorded for an additional 100 steps, yielding $100 \text{ steps} \times 400 \text{ walkers} = 40,000$ samples for each parameter at each temperature. Chains were assessed for mixing by inspection of the posteriors associated with the positions of each walker across a subset of temperatures. The frequency of accepted temperature swaps was also inspected to ensure proper mixing between chains at different temperatures. Sampling runs were performed primarily on a computing cluster assembled from Amazon Elastic Compute Cloud (EC2) instances using the StarCluster software package⁶³. All code necessary to reproduce the results of data analysis and model calibration is freely available on GitHub, at https://github.com/johnbachman/bax_insertion_paper.

References

1. Youle, R.J. & Strasser, A. The BCL-2 protein family: opposing activities that mediate cell death. *Nat Rev Mol Cell Biol* **9**, 47-59 (2008).
2. Kale, J., Osterlund, E.J. & Andrews, D.W. BCL-2 family proteins: changing partners in the dance towards death. *Cell Death Differ* **25**, 65-80 (2018).

3. Kroemer, G., Galluzzi, L. & Brenner, C. Mitochondrial membrane permeabilization in cell death. *Physiol Rev* **87**, 99-163 (2007).
4. Tait, S.W. & Green, D.R. Mitochondria and cell death: outer membrane permeabilization and beyond. *Nat Rev Mol Cell Biol* **11**, 621-32 (2010).
5. Goldstein, J.C., Waterhouse, N.J., Juin, P., Evan, G.I. & Green, D.R. The coordinate release of cytochrome c during apoptosis is rapid, complete and kinetically invariant. *Nat Cell Biol* **2**, 156-62 (2000).
6. Rehm, M. et al. Single-cell fluorescence resonance energy transfer analysis demonstrates that caspase activation during apoptosis is a rapid process. Role of caspase-3. *J Biol Chem* **277**, 24506-14 (2002).
7. Albeck, J.G., Burke, J.M., Spencer, S.L., Lauffenburger, D.A. & Sorger, P.K. Modeling a snap-action, variable-delay switch controlling extrinsic cell death. *PLoS Biol* **6**, 2831-52 (2008).
8. Aouacheria, A., Combet, C., Tompa, P. & Hardwick, J.M. Redefining the BH3 Death Domain as a 'Short Linear Motif'. *Trends Biochem Sci* **40**, 736-748 (2015).
9. Bleicken, S. et al. Topology of active, membrane-embedded Bax in the context of a toroidal pore. *Cell Death Differ* **25**, 1717-1731 (2018).
10. Czabotar, P.E. et al. Bax crystal structures reveal how BH3 domains activate Bax and nucleate its oligomerization to induce apoptosis. *Cell* **152**, 519-31 (2013).
11. Bleicken, S. et al. Structural model of active Bax at the membrane. *Mol Cell* **56**, 496-505 (2014).
12. Zhang, Z. et al. BH3-in-groove dimerization initiates and helix 9 dimerization expands Bax pore assembly in membranes. *EMBO J* **35**, 208-36 (2016).
13. Flores-Romero, H., Garcia-Porras, M. & Basanez, G. Membrane insertion of the BAX core, but not latch domain, drives apoptotic pore formation. *Sci Rep* **7**, 16259 (2017).
14. Saito, M., Korsmeyer, S.J. & Schlesinger, P.H. BAX-dependent transport of cytochrome c reconstituted in pure liposomes. *Nat Cell Biol* **2**, 553-5 (2000).
15. Lovell, J.F. et al. Membrane binding by tBid initiates an ordered series of events culminating in membrane permeabilization by Bax. *Cell* **135**, 1074-84 (2008).
16. Kushnareva, Y., Andreyev, A.Y., Kuwana, T. & Newmeyer, D.D. Bax activation initiates the assembly of a multimeric catalyst that facilitates Bax pore formation in mitochondrial outer membranes. *PLoS Biol* **10**, e1001394 (2012).
17. Kale, J., Chi, X., Leber, B. & Andrews, D. Examining the molecular mechanism of bcl-2 family proteins at membranes by fluorescence spectroscopy. *Methods Enzymol* **544**, 1-23 (2014).
18. Rojko, N. et al. Membrane damage by an alpha-helical pore-forming protein, Equinatoxin II, proceeds through a succession of ordered steps. *J Biol Chem* **288**, 23704-15 (2013).
19. Shamas-Din, A. et al. tBid undergoes multiple conformational changes at the membrane required for Bax activation. *J Biol Chem* **288**, 22111-27 (2013).
20. Gelman, A. Bayesian data analysis. *Chapman & Hall/CRC texts in statistical science*, xiv, 661 pages (2014).
21. Annis, M.G. et al. Bax forms multispinning monomers that oligomerize to permeabilize membranes during apoptosis. *EMBO Journal* **24**, 2096-103 (2005).

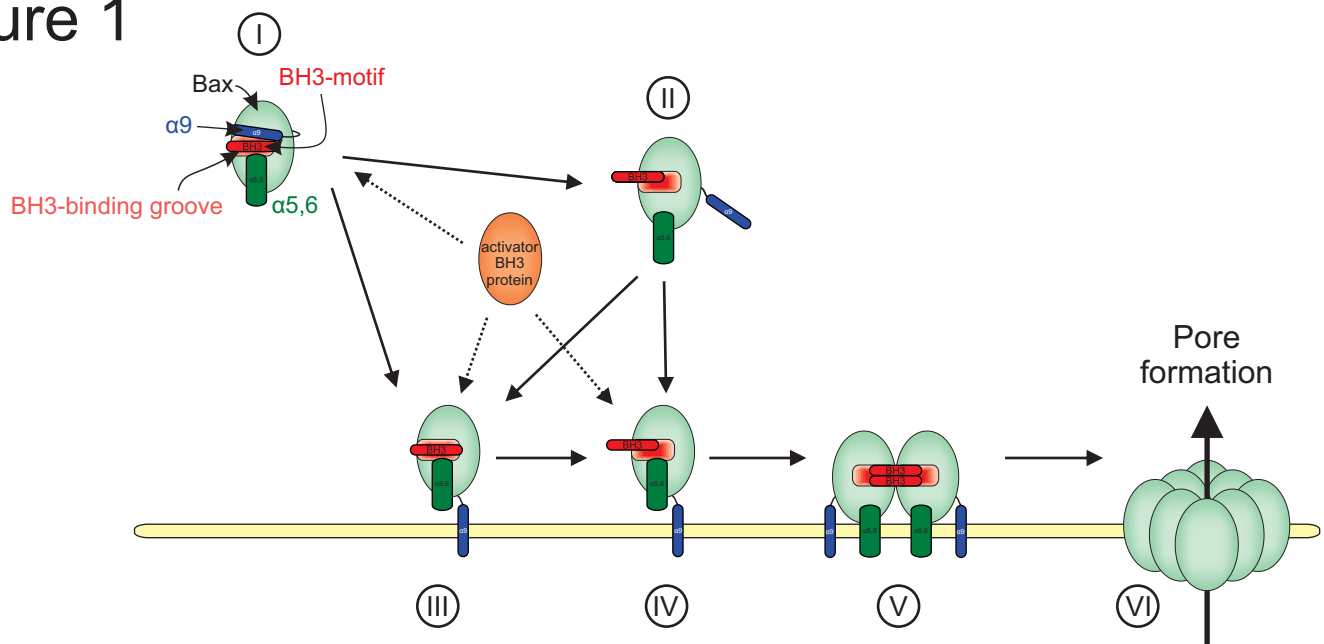
22. Westphal, D. et al. Apoptotic pore formation is associated with in-plane insertion of Bak or Bax central helices into the mitochondrial outer membrane. *Proc Natl Acad Sci U S A* **111**, E4076-85 (2014).
23. Yethon, J.A., Epand, R.F., Leber, B., Epand, R.M. & Andrews, D.W. Interaction with a membrane surface triggers a reversible conformational change in Bax normally associated with induction of apoptosis. *J Biol Chem* **278**, 48935-41 (2003).
24. Dengler, M.A. et al. BAX Activation: Mutations Near Its Proposed Non-canonical BH3 Binding Site Reveal Allosteric Changes Controlling Mitochondrial Association. *Cell Rep* **27**, 359-373 e6 (2019).
25. Gavathiotis, E. et al. BAX activation is initiated at a novel interaction site. *Nature* **455**, 1076-81 (2008).
26. Robin, A.Y. et al. Crystal structure of Bax bound to the BH3 peptide of Bim identifies important contacts for interaction. *Cell Death Dis* **6**, e1809 (2015).
27. Yin, C., Knudson, C.M., Korsmeyer, S.J. & Van Dyke, T. Bax suppresses tumorigenesis and stimulates apoptosis in vivo. *Nature* **385**, 637-40 (1997).
28. Hanahan, D. & Weinberg, R.A. Hallmarks of cancer: the next generation. *Cell* **144**, 646-74 (2011).
29. Cerami, E. et al. The cBio cancer genomics portal: an open platform for exploring multidimensional cancer genomics data. *Cancer Discov* **2**, 401-4 (2012).
30. Gao, J. et al. Integrative analysis of complex cancer genomics and clinical profiles using the cBioPortal. *Sci Signal* **6**, p11 (2013).
31. Nechushtan, A., Smith, C.L., Hsu, Y.T. & Youle, R.J. Conformation of the Bax C-terminus regulates subcellular location and cell death. *EMBO Journal* **18**, 2330-2341 (1999).
32. Meijerink, J.P. et al. Hematopoietic malignancies demonstrate loss-of-function mutations of BAX. *Blood* **91**, 2991-7 (1998).
33. Kim, H. et al. Stepwise activation of BAX and BAK by tBID, BIM, and PUMA initiates mitochondrial apoptosis. *Mol Cell* **36**, 487-99 (2009).
34. Fresquet, V., Rieger, M., Carolis, C., Garcia-Barchino, M.J. & Martinez-Climent, J.A. Acquired mutations in BCL2 family proteins conferring resistance to the BH3 mimetic ABT-199 in lymphoma. *Blood* **123**, 4111-9 (2014).
35. Kale, J. et al. Phosphorylation switches Bax from promoting to inhibiting apoptosis thereby increasing drug resistance. *EMBO Rep* (2018).
36. Chi, X. et al. The carboxyl-terminal sequence of Bim enables Bax activation and killing of unprimed cells. *bioRxiv*, 554907 (2019).
37. Dai, H. et al. Transient binding of an activator BH3 domain to the Bak BH3-binding groove initiates Bak oligomerization. *J Cell Biol* **194**, 39-48 (2011).
38. Dewson, G. et al. Bax dimerizes via a symmetric BH3:groove interface during apoptosis. *Cell Death Differ* **19**, 661-70 (2012).
39. Subburaj, Y. et al. Bax monomers form dimer units in the membrane that further self-assemble into multiple oligomeric species. *Nat Commun* **6**, 8042 (2015).
40. Tsai, C.J. et al. BAX-induced apoptosis can be initiated through a conformational selection mechanism. *Structure* **23**, 139-48 (2015).
41. Suzuki, M., Youle, R.J. & Tjandra, N. Structure of Bax: coregulation of dimer formation and intracellular localization. *Cell* **103**, 645-54 (2000).

42. Dewson, G. et al. To trigger apoptosis, Bak exposes its BH3 domain and homodimerizes via BH3:groove interactions. *Mol Cell* **30**, 369-80 (2008).
43. Gavathiotis, E., Reyna, D.E., Davis, M.L., Bird, G.H. & Walensky, L.D. BH3-triggered structural reorganization drives the activation of proapoptotic BAX. *Mol Cell* **40**, 481-92 (2010).
44. Garner, T.P. et al. An Autoinhibited Dimeric Form of BAX Regulates the BAX Activation Pathway. *Mol Cell* **63**, 485-97 (2016).
45. Cosentino, K. & Garcia-Saez, A.J. Bax and Bak Pores: Are We Closing the Circle? *Trends Cell Biol* **27**, 266-275 (2017).
46. Galluzzi, L. et al. Essential versus accessory aspects of cell death: recommendations of the NCCD 2015. *Cell Death Differ* **22**, 58-73 (2015).
47. Niu, X. et al. A Small-Molecule Inhibitor of Bax and Bak Oligomerization Prevents Genotoxic Cell Death and Promotes Neuroprotection. *Cell Chem Biol* **24**, 493-506 e5 (2017).
48. Garner, T.P. et al. Small-molecule allosteric inhibitors of BAX. *Nat Chem Biol* (2019).
49. Brouwer, J.M. et al. Conversion of Bim-BH3 from Activator to Inhibitor of Bak through Structure-Based Design. *Mol Cell* **68**, 659-672 e9 (2017).
50. Li, R. et al. Modulation of Bax and mTOR for Cancer Therapeutics. *Cancer Res* **77**, 3001-3012 (2017).
51. Pritz, J.R. et al. Allosteric sensitization of proapoptotic BAX. *Nat Chem Biol* **13**, 961-967 (2017).
52. Adams, J.M. & Cory, S. The BCL-2 arbiters of apoptosis and their growing role as cancer targets. *Cell Death Differ* **25**, 27-36 (2018).
53. Birkinshaw, R.W. & Czabotar, P.E. The BCL-2 family of proteins and mitochondrial outer membrane permeabilisation. *Semin Cell Dev Biol* (2017).
54. Sarosiek, K.A. et al. BID preferentially activates BAK while BIM preferentially activates BAX, affecting chemotherapy response. *Mol Cell* **51**, 751-65 (2013).
55. Shamas-Din, A. et al. Multiple partners can kiss-and-run: Bax transfers between multiple membranes and permeabilizes those primed by tBid. *Cell Death Dis* **5**, e1277 (2014).
56. Lopez, C.F., Muhlich, J.L., Bachman, J.A. & Sorger, P.K. Programming biological models in Python using PySB. *Mol Syst Biol* **9**, 646 (2013).
57. Brown, P.N., Byrne, G.D. & Hindmarsh, A.C. VODE, A variable coefficient ODE solver. *SIAM J Sci Stat Comput* **10**, 1038-1051 (1989).
58. Oliphant, T.E. Python for Scientific Computing. *Computing in Science & Engineering* **9**, 10-20 (2007).
59. Foreman-Mackey, D., Hogg, D.W., Lang, D. & Goodman, J. emcee: The MCMC Hammer. *Publications of the Astronomical Society of the Pacific* **125**, 306-312 (2013).
60. Goodman, J. & Weare, J. Ensemble samplers with affine invariance. *Communications in Applied Mathematics and Computational Science* **5**, 65-80 (2010).
61. Geyer, C.J. Markov chain Monte Carlo maximum likelihood. *Computing Science and Statistics: Proc. 23rd Symposium on the Interface, Interface Foundation, Fairfax Station, VA*, 156-163 (1991).
62. Lartillot, N. & Hervé, P. Computing Bayes factors using thermodynamic integration. *Systematic Biology* **55**, 195-207 (2006).

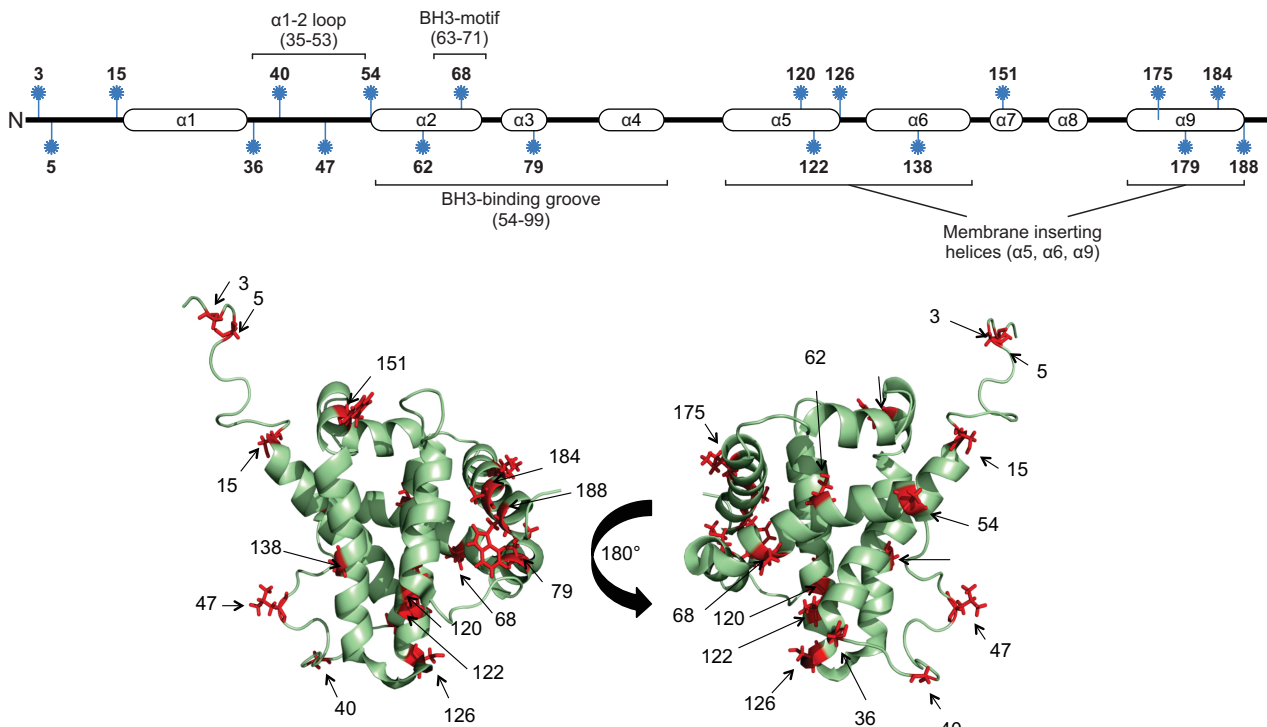
63. Fusaro, V.A., Patil, P., Gafni, E., Wall, D.P. & Tonellato, P.J. Biomedical cloud computing with Amazon Web Services. *PLoS Comput Biol* **7**, e1002147 (2011).

Figure 1

a



b



c

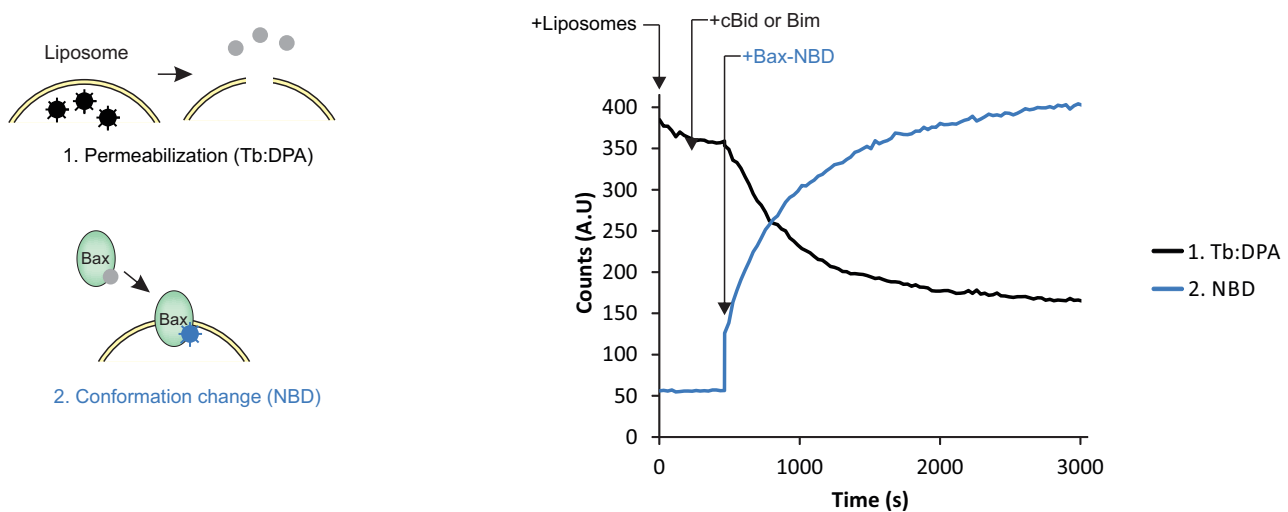
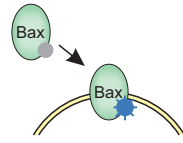
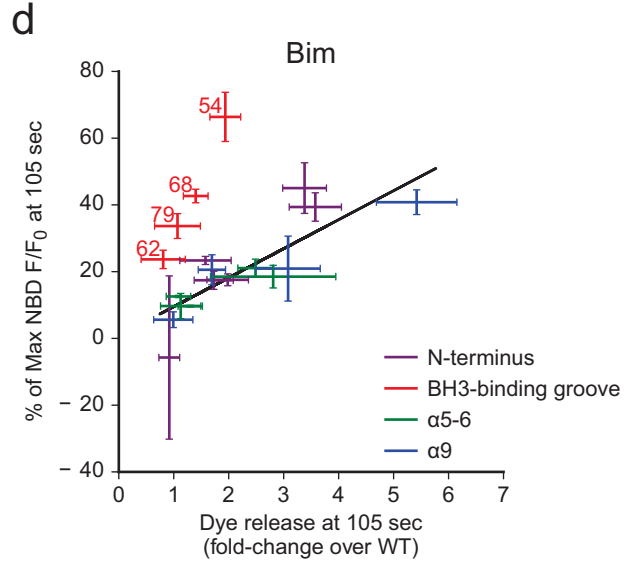
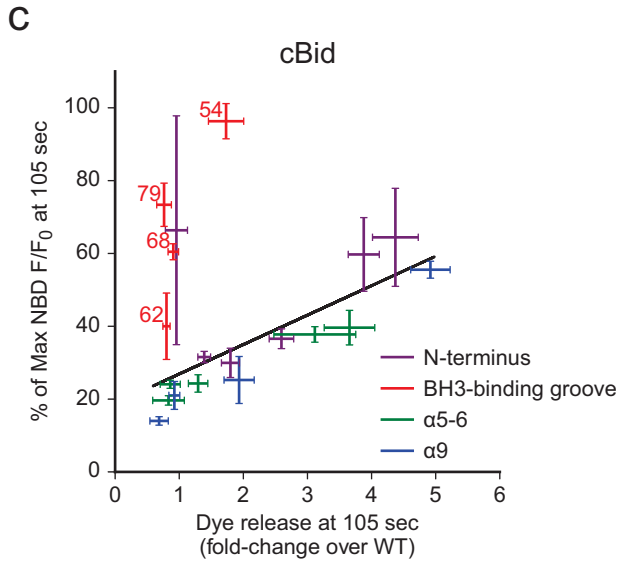
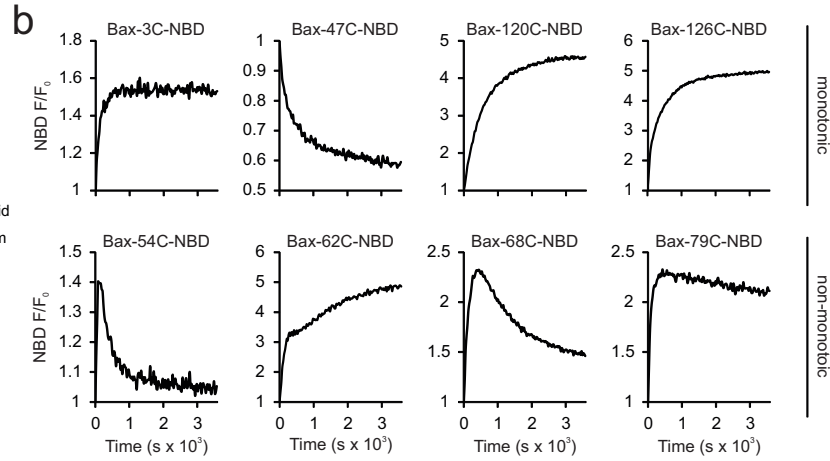
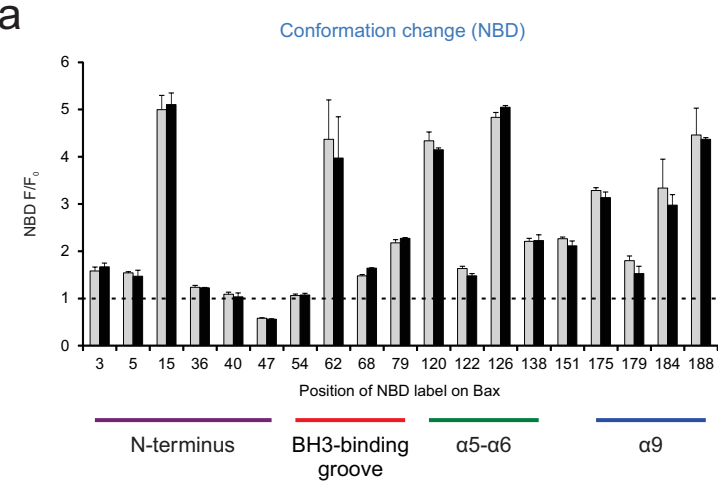


Figure 2



Conformation change (NBD)



S1

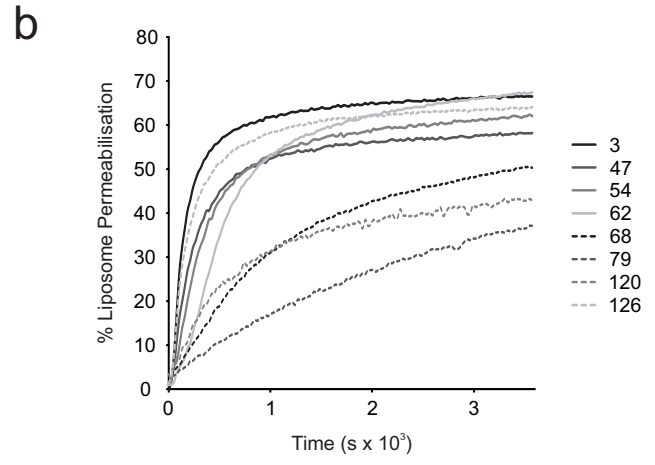
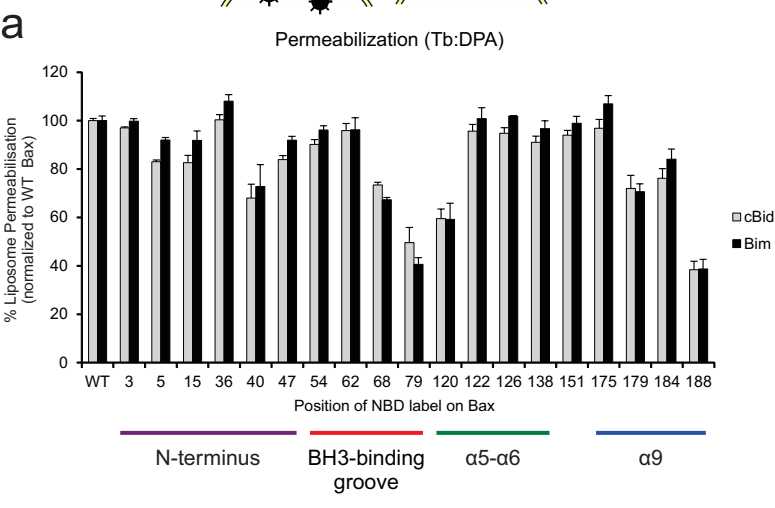
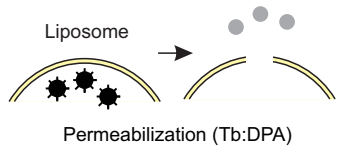


Figure 3

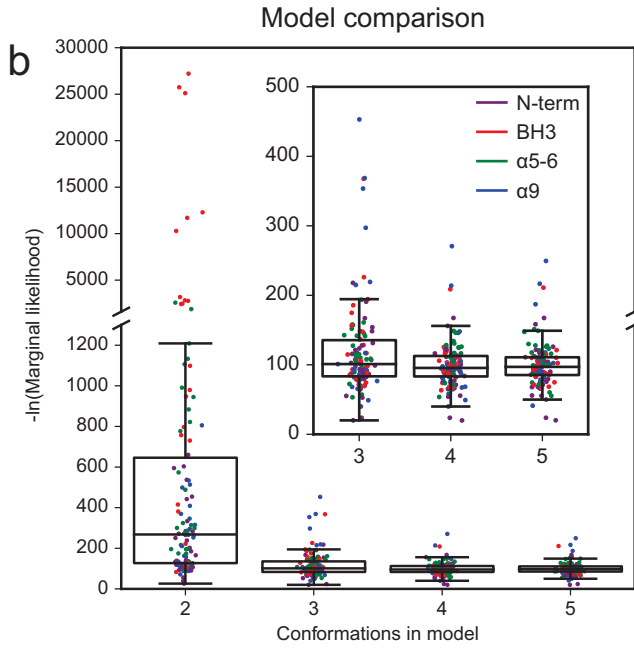
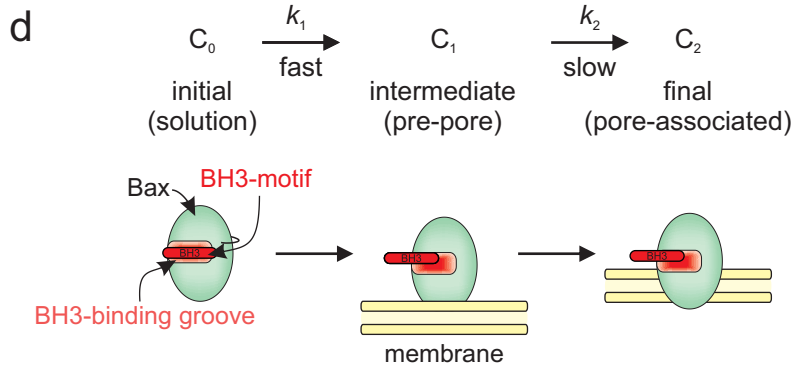
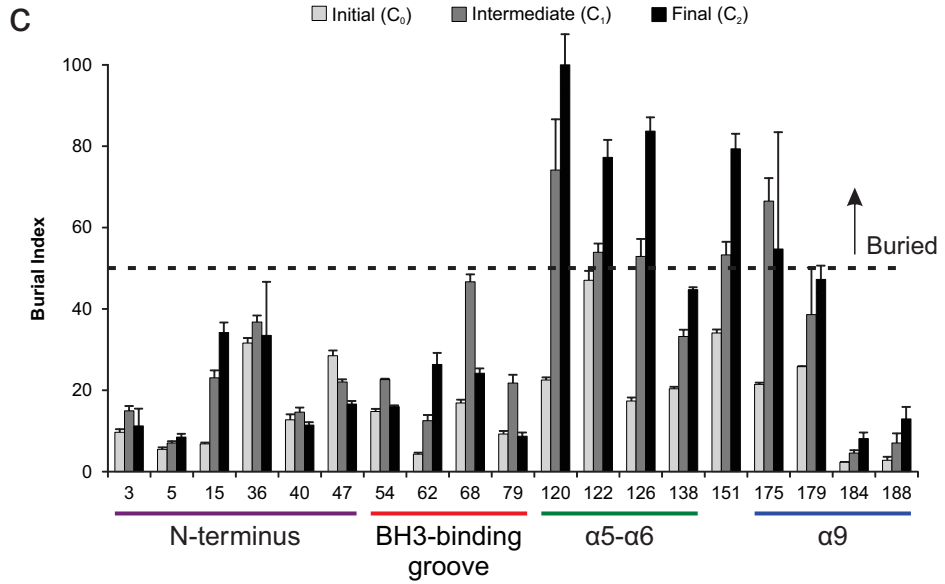
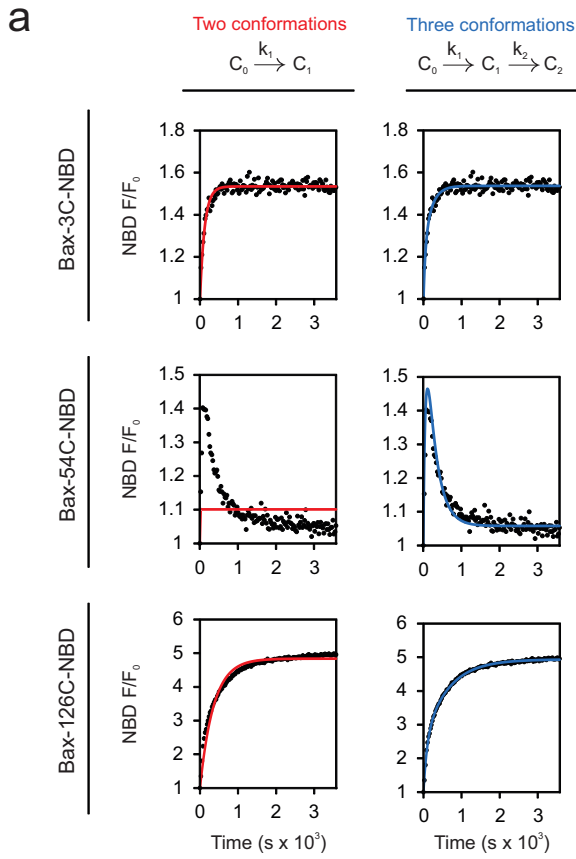


Figure S2

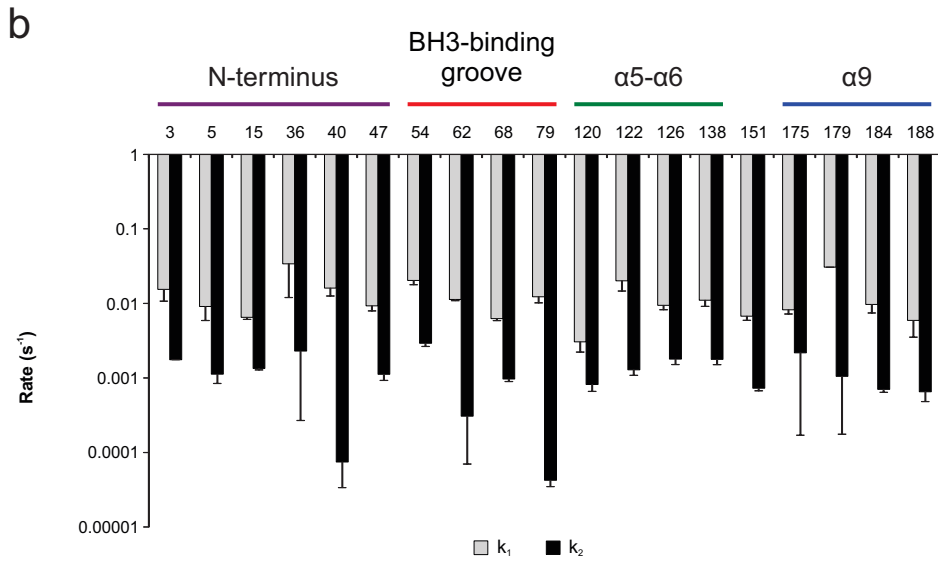
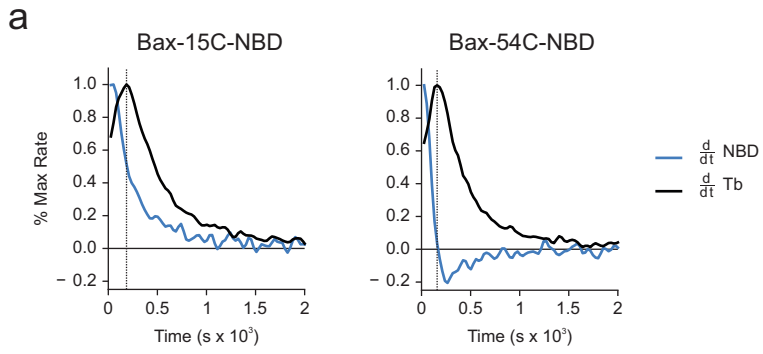
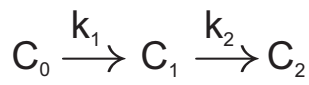
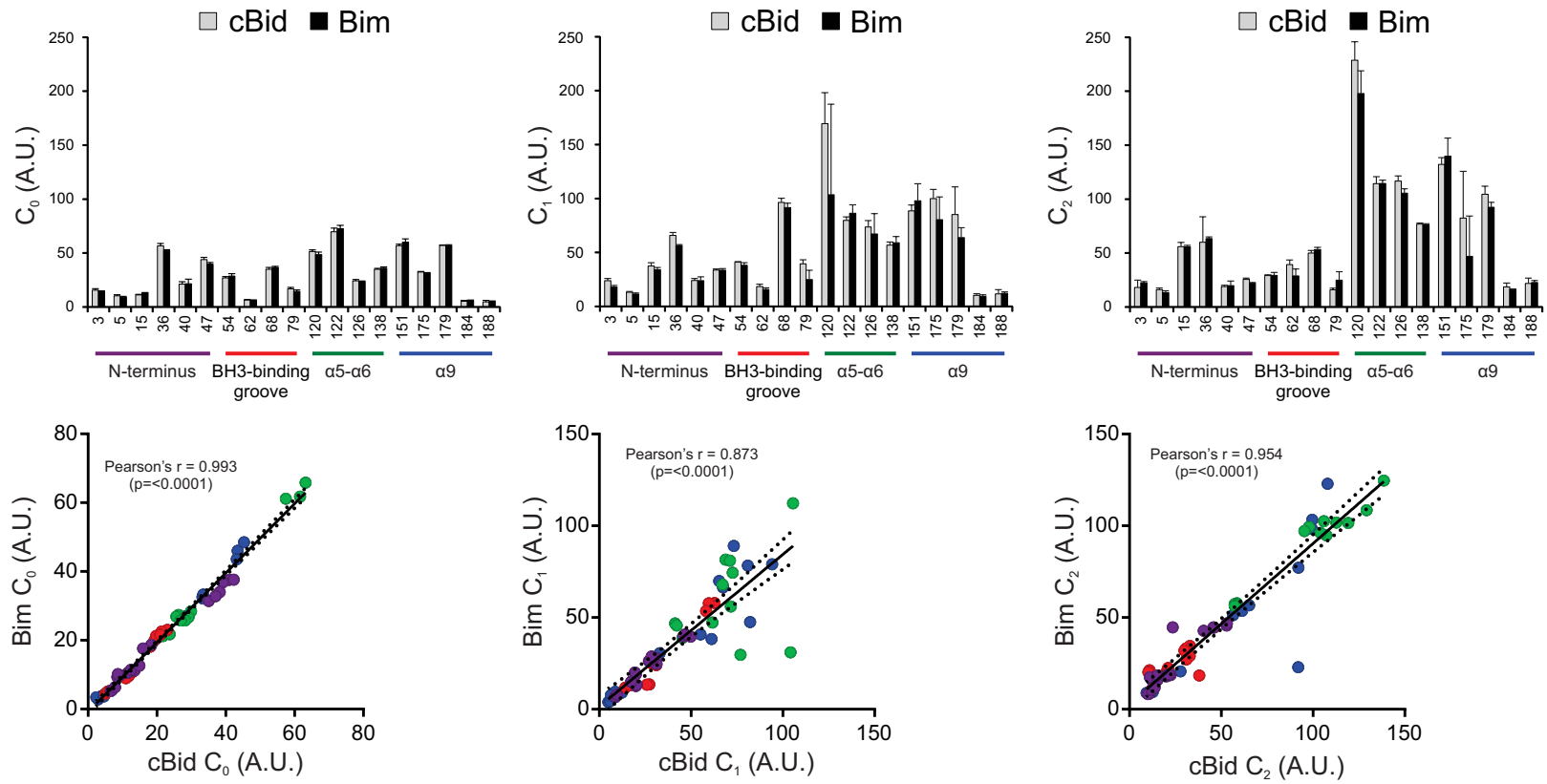


Figure 4



a



b

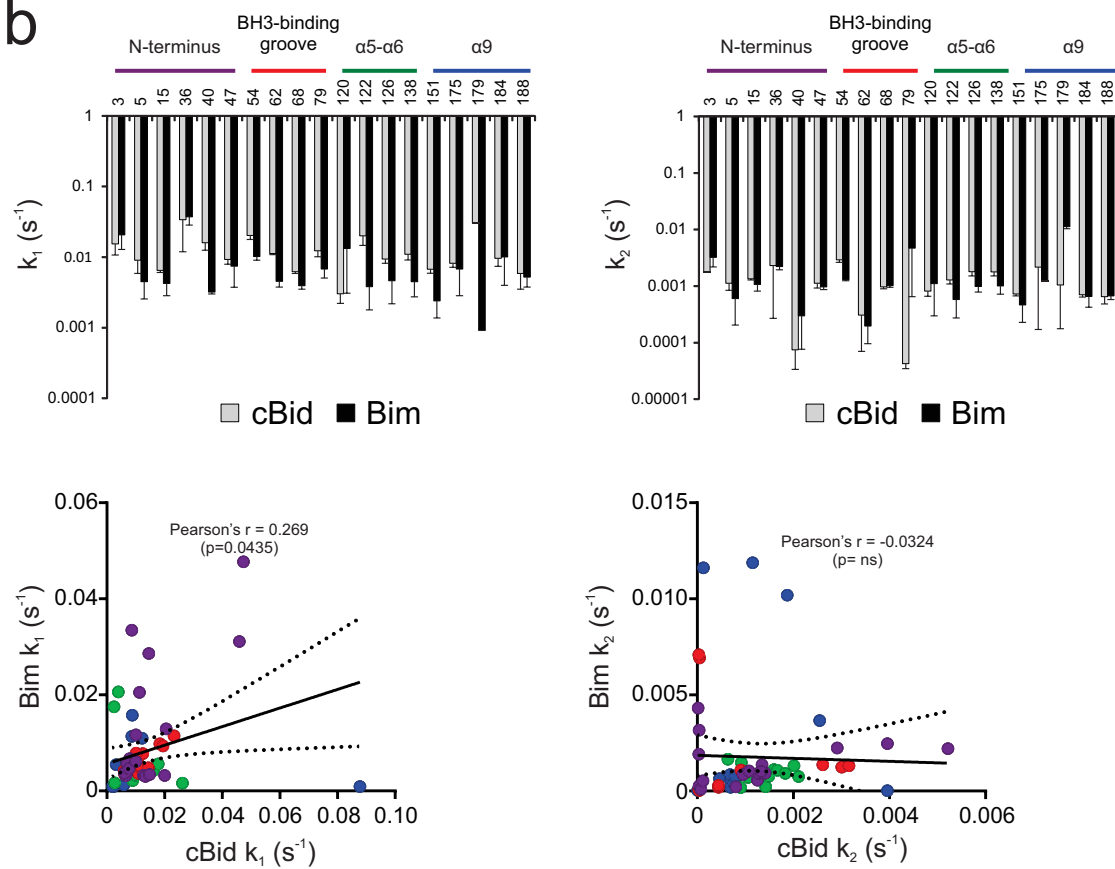


Figure 5

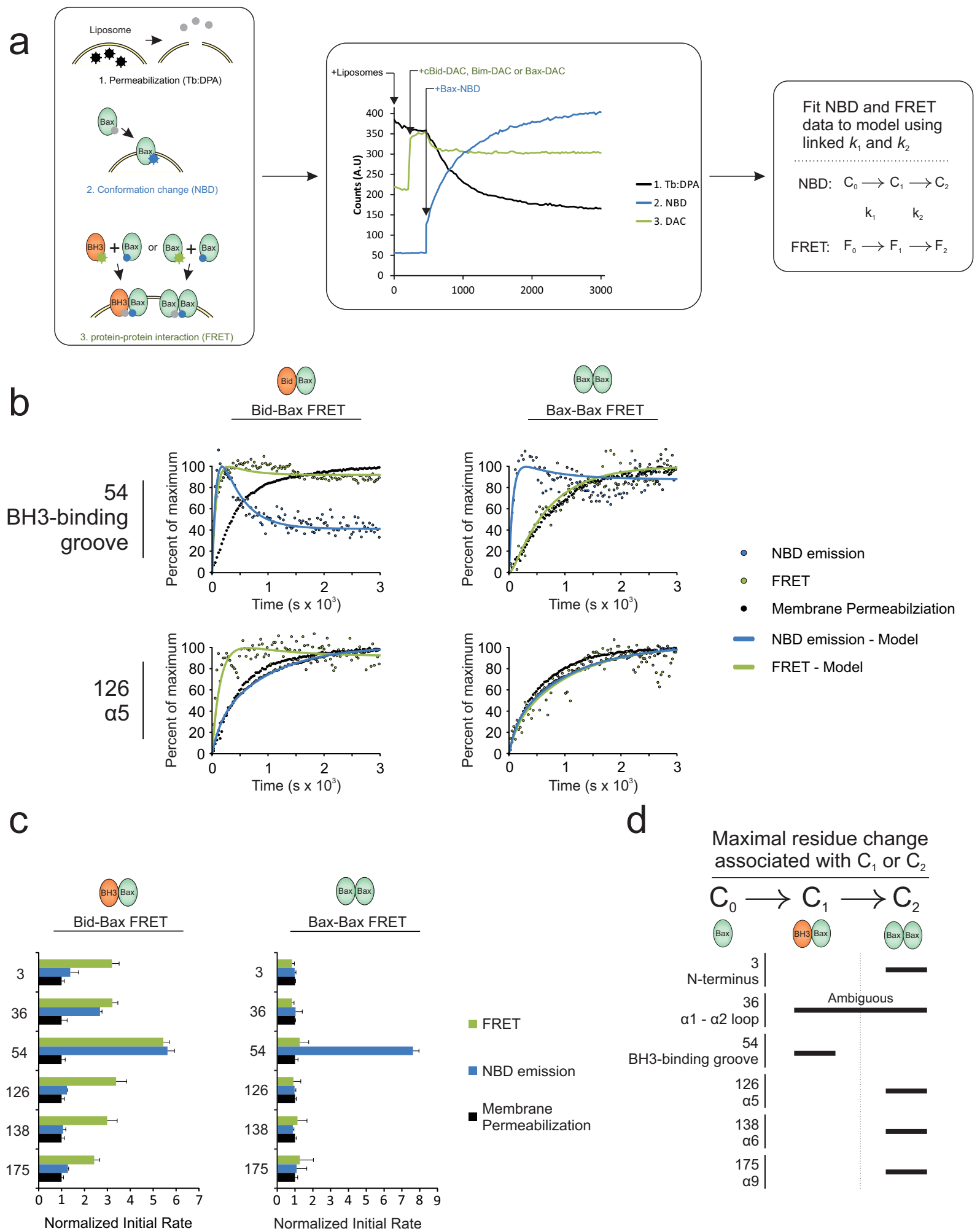
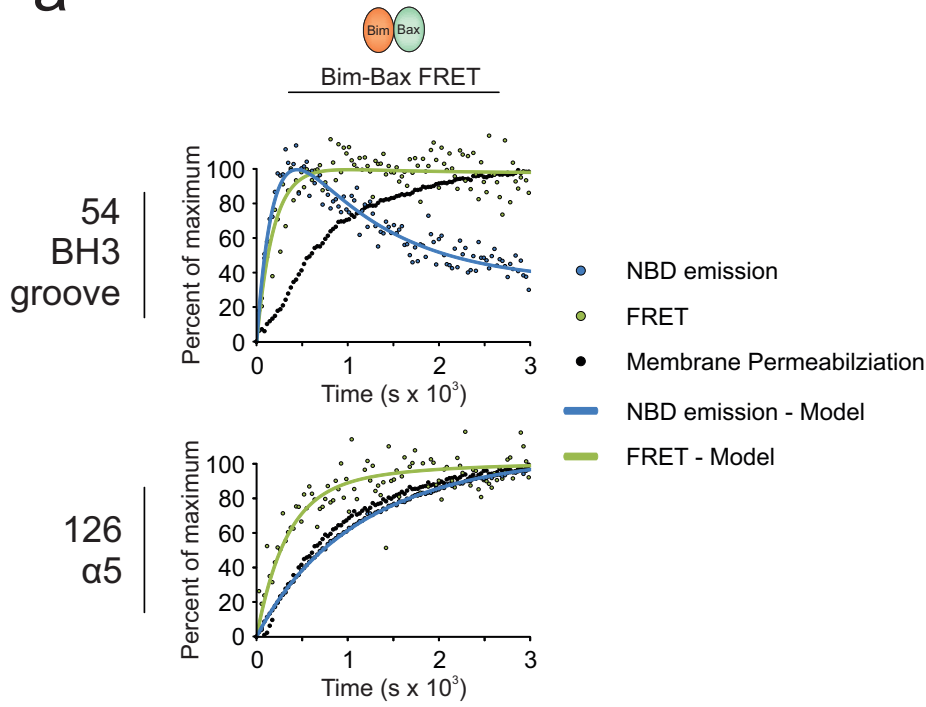
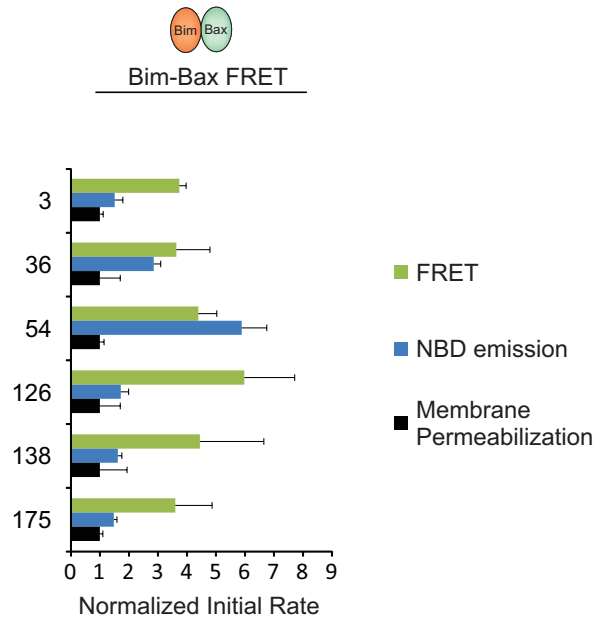


Figure S3

a



b



c

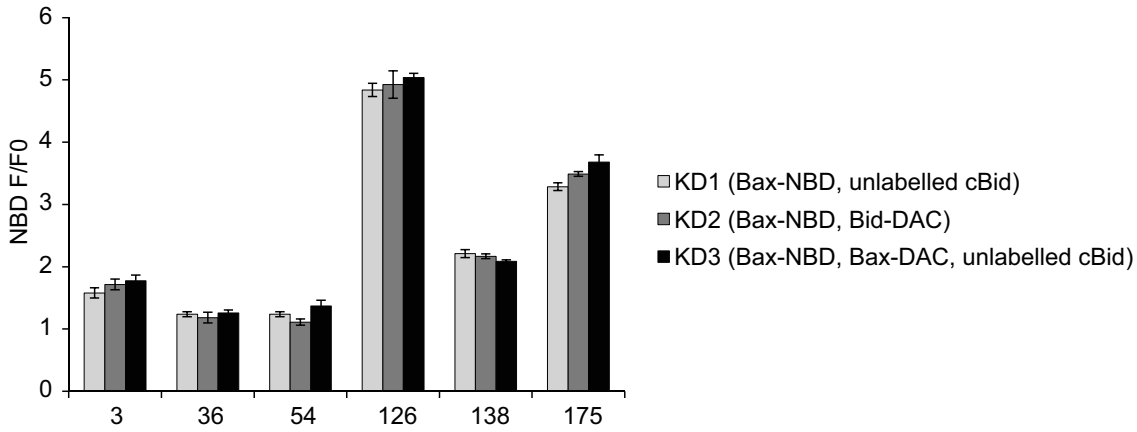


Figure 6

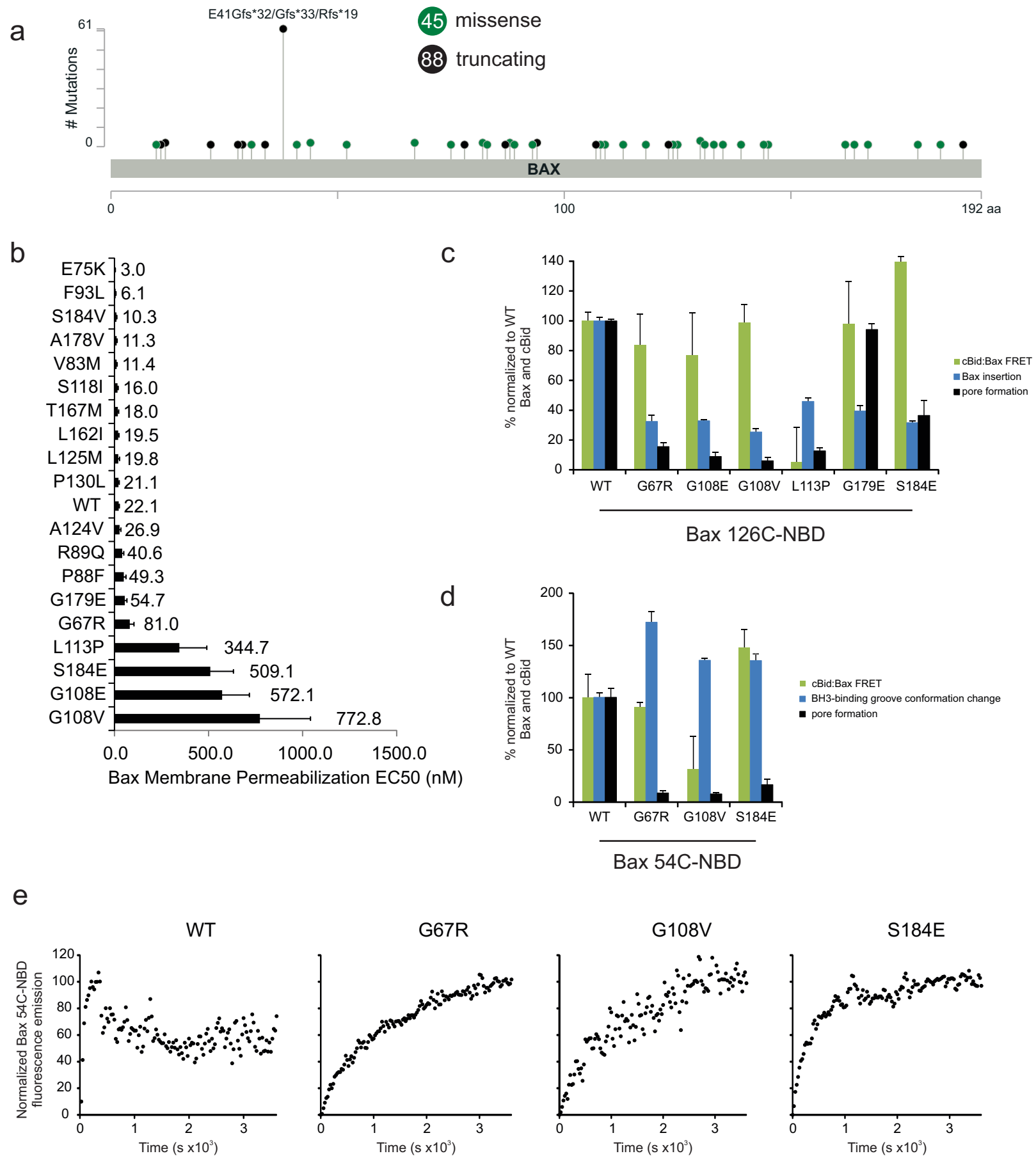


Figure 7

